bioRxiv preprint doi: https://doi.org/10.1101/372300; this version posted December 8, 2018. The copyright holder for this preprint (which was not certified by peer review) is the author/funder, who has granted bioRxiv a license to display the preprint in perpetuity. It is made available under aCC-BY 4.0 International license.

The architecture of functional lateralisation and its relationship to callosal connectivity in the human brain

Karolis VR [a,b*], Corbetta M [c-g] & Thiebaut de Schotten M [a,b,h*]

[a] Brain Connectivity and Behaviour Group, Sorbonne Universities, Paris France.

[b] Frontlab, Institut du Cerveau et de la Moelle épinière (ICM), UPMC UMRS 1127, Inserm U 1127, CNRS UMR 7225, Paris, France.

[c] Department of Neuroscience, University of Padova, Italy

[d] Padova Neuroscience Center (PNC), University of Padova, Italy

[e] Department of Neurology, Washington University Saint Louis, USA

[f] Department of Radiology, Washington University Saint Louis, USA c Department of Neuroscience, Washington University Saint Louis, USA

[g] Department of Biomedical Engineering, Washington University Saint Louis, USA

[h] Groupe d'Imagerie Neurofonctionnelle, Institut des Maladies Neurodégénératives-UMR 5293, CNRS, CEA University of Bordeaux, Bordeaux, France

* Corresponding authors slava.karolis@kcl.ac.uk and michel.thiebaut@gmail.com

bioRxiv preprint doi: https://doi.org/10.1101/372300; this version posted December 8, 2018. The copyright holder for this preprint (which was not certified by peer review) is the author/funder, who has granted bioRxiv a license to display the preprint in perpetuity. It is made available under aCC-BY 4.0 International license.

Abstract

Functional lateralisation is a fundamental principle of the human brain. However, a comprehensive taxonomy of functional lateralisation and its organisation in the brain is missing. We report the first complete map of functional hemispheric asymmetries in the human brain, reveal its low dimensional structure, and its relationship with structural inter-hemispheric connectivity. Our results suggest that the lateralisation of brain functions is distributed along four functional axes: symbolic communication, perception/action, emotion, and decision-making, and that cortical regions showing asymmetries in task-evoked activity have reduced connections with the opposite hemisphere.

bioRxiv preprint doi: https://doi.org/10.1101/372300; this version posted December 8, 2018. The copyright holder for this preprint (which was not certified by peer review) is the author/funder, who has granted bioRxiv a license to display the preprint in perpetuity. It is made available under aCC-BY 4.0 International license.

"Are you left- or right-brain?". The widespread belief that hemispheric dominance influences the human character comes from a misinterpretation of several decades of neuropsychological findings [1] that show that functional lateralisation is a fundamental principle of the brain's organisation [2, 3, 4]. Today, after nearly 30 years of functional neuroimaging, theories on functional lateralisation suggest a less radical division and assume that the two hemispheres balance one another [5]. However, despite the implications of functional lateralisation theories for neurodevelopmental and psychiatric disorders [6, 7], as well as for stroke recovery [8, 9, 10, 11], a comprehensive mapping of functional lateralisation in the brain is, to our knowledge, still missing in the literature. It is also not known whether putatively lateralised cognitive functions share similar or different spatial patterns of functional activation and whether these functional activations can be categorised to a limited number of spatial patterns—have a low dimensional structure.

Furthermore, the mechanisms that sustain functional lateralisation, and related inter-hemispheric communication, remain debated [12, 13]. Two competing hypotheses have been proposed on the emergence of functional lateralisation based on the structure of the corpus callosum, the most considerable inter-hemispheric connection. The *inter-hemispheric independence* hypothesis suggests that, during evolution, brain size expansion led to functional lateralisation in order to avoid excessive conduction delays between the hemispheres[14]. Accordingly, functionally lateralised regions will be connected less strongly via the corpus callosum than non-lateralised regions to make processing of lateralized functions more efficient [15]. The *inter-hemispheric competition* hypothesis proposes that functional lateralisation arises from the competition between the hemispheres that inhibit each other via the corpus callosum. As functionally lateralised regions would need to inhibit the opposite hemisphere more than non-lateralised regions, they could be more connected by the corpus callosum. Preliminary anatomical [16] and fMRI [17] studies provide support for both theories. However, the small range of functions investigated and shortcomings in the methods often limit the interpretability of the findings [13]. Overall, the generalisation of these theories and findings to the whole brain's functional organisation remains unknown.

Here, we took advantage of combining the largest fMRI meta-analytic dataset [18] with the highest quality structural connectivity data [19] to produce, for the first time, a comprehensive map of the functional brain architecture of lateralized cognitive functions, characterise its low dimensional structure, and examine its relationship to corpus callosum connectivity.

bioRxiv preprint doi: https://doi.org/10.1101/372300; this version posted December 8, 2018. The copyright holder for this preprint (which was not certified by peer review) is the author/funder, who has granted bioRxiv a license to display the preprint in perpetuity. It is made available under aCC-BY 4.0 International license.

Results

Functional lateralisation maps and their low-dimensional structure

We selected 590 terms related to specific cognitive processes out of the whole Neurosynth database (see **Supplementary Table 1**). A functional lateralisation map was computed for each term by calculating the difference between hemispheres for each pair of homologous voxels. Homologous functional regions may be displaced in the two hemispheres because of anatomical factors, e.g. the Yakovlevian torque [4, 20], the size of the planum temporale [21] and motor cortex [22, 23] , or functional factors, e.g. the way perception and action are coupled in each hemisphere [24, 25]. Here we adjusted for main anatomical asymmetries in the two hemispheres by registering the maps to a symmetric atlas [26].

We first sought to determine which regions show a significant functional lateralisation. Given that selected terms could be either correlated or related in a trivial way (e.g., singular and plural forms of the same word; "visual form" and "visual forms"), a varimax-rotated principal component analysis was run in order to eliminate redundancy in the data. 171 principal components with eigenvalues higher than the grand average were retained, explaining 72.6% of the variance of the lateralisation maps. General linear modelling was subsequently employed with component loads as a set of predictors to fit lateralisation maps data and identify voxels with a significant lateralisation associated with each component. After 5000 permutations, 25 principal components showed voxels with a significant lateralisation (>20 voxels; $P < 0.05$ family-wise error corrected; see **Supplementary Table 2**). Essentially, these represent the significant groups of voxels showing significant functional lateralisation in Neurosynth.

Next, a multivariate spectral embedding, based on the similarity between lateralisation maps, enabled us to examine a generic structure of the brain's functional lateralisation profiles, i.e. its "morphospace" [27, 28]. The preliminary step that included the embedding in the first two dimensions (**Figure 1a** and **Supplementary Figure 1**) revealed a triangular organisation of the lateralisation maps with three vertices: symbolic communication, perception/action, and emotion. A t-ratio test, i.e. a test of pareto optimality [29], between the organisation of real data and 2000 samples of simulated data, which were obtained via permutations of the voxel order before computing right-left differences, confirmed the statistical veracity of such triangular organisation. The same analysis was used to explore other dimensions and revealed three

bioRxiv preprint doi: https://doi.org/10.1101/372300; this version posted December 8, 2018. The copyright holder for this preprint (which was not certified by peer review) is the author/funder, who has granted bioRxiv a license to display the preprint in perpetuity. It is made available under aCC-BY 4.0 International license.

additional triangles and a 4th vertex given by decision making. (**Figure 1b** and **Supplementary Figure 2**).

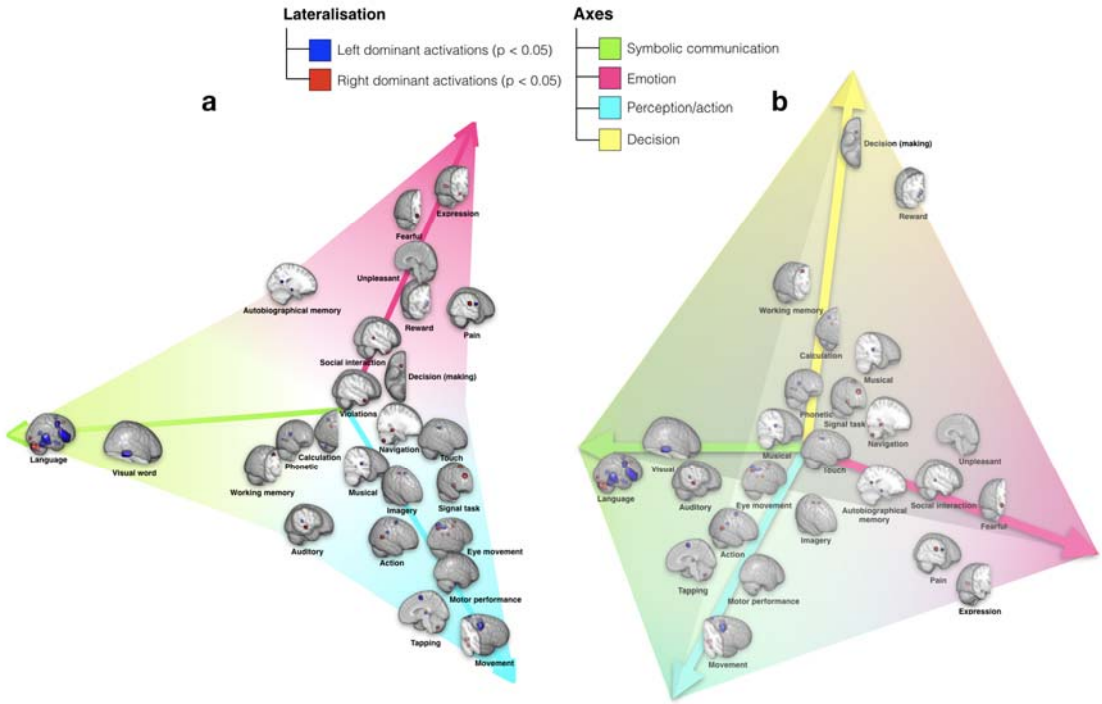

Figure 1. Low dimensional structure of functionally lateralised regions in the brain embedded in two- (**a**) and three- (**b**) dimensional space according to similarity in their lateralisation profile. See **Supplementary Figure 1 and 2** for the spatial embedding of all Neurosynth terms. Here, to provide a graphical summary of all results reported in the section, we plotted the significantly lateralised components maps, named by the highest-loading terms (**Supplementary Table 3**), in place of the actual Neurosynth terms (**Supplementary Table 1**).

Furthermore, by regressing lateralisation profiles onto terms' coordinates in the embedded space, we constructed predictions for the maps located at the coordinates of the vertices, which we will refer to as archetype maps.

The archetype maps corresponding to the symbolic communication axis was characterised by a left dominant activation of the dorsal and ventral posterior part of the frontal lobe, including Broca area and the pre-supplementary motor area, the posterior part of the temporal lobe, including Wernicke area and the Visual Word Form Area (i.e. VWFA). Right dominant

bioRxiv preprint doi: https://doi.org/10.1101/372300; this version posted December 8, 2018. The copyright holder for this preprint (which was not certified by peer review) is the author/funder, who has granted bioRxiv a license to display the preprint in perpetuity. It is made available under aCC-BY 4.0 International license.

activations were located in the posterior lobe of the cerebellum, including area Crus II (**Figure 2a**).

The archetype perception/action map involved left sensorimotor cortex, left SMA, and left thalamus. Right dominant activations included frontal eye field, intraparietal region, and ventral frontal regions, frontal eye field, pre-supplementary motor area, basal forebrain and anterior cerebellum (i.e. Areas V/VI and VIII) as well as part of the vermis (**Figure 2b**).

The archetype emotion map involved the left anterior cingulate cortex, the basolateral complex of the right amygdala, the posterior part of the right inferior frontal gyrus, the right intraparietal sulcus and the posterior part of the right temporal lobe (**Figure 2c**).

Finally, the decision-making archetype map involved mostly the right prefrontal cortex (i.e. medial orbital gyrus), the right frontal eye field, the left intraparietal sulcus together with the striatum (right putamen and left caudate) and the left basal forebrain (**Figure 2d**).

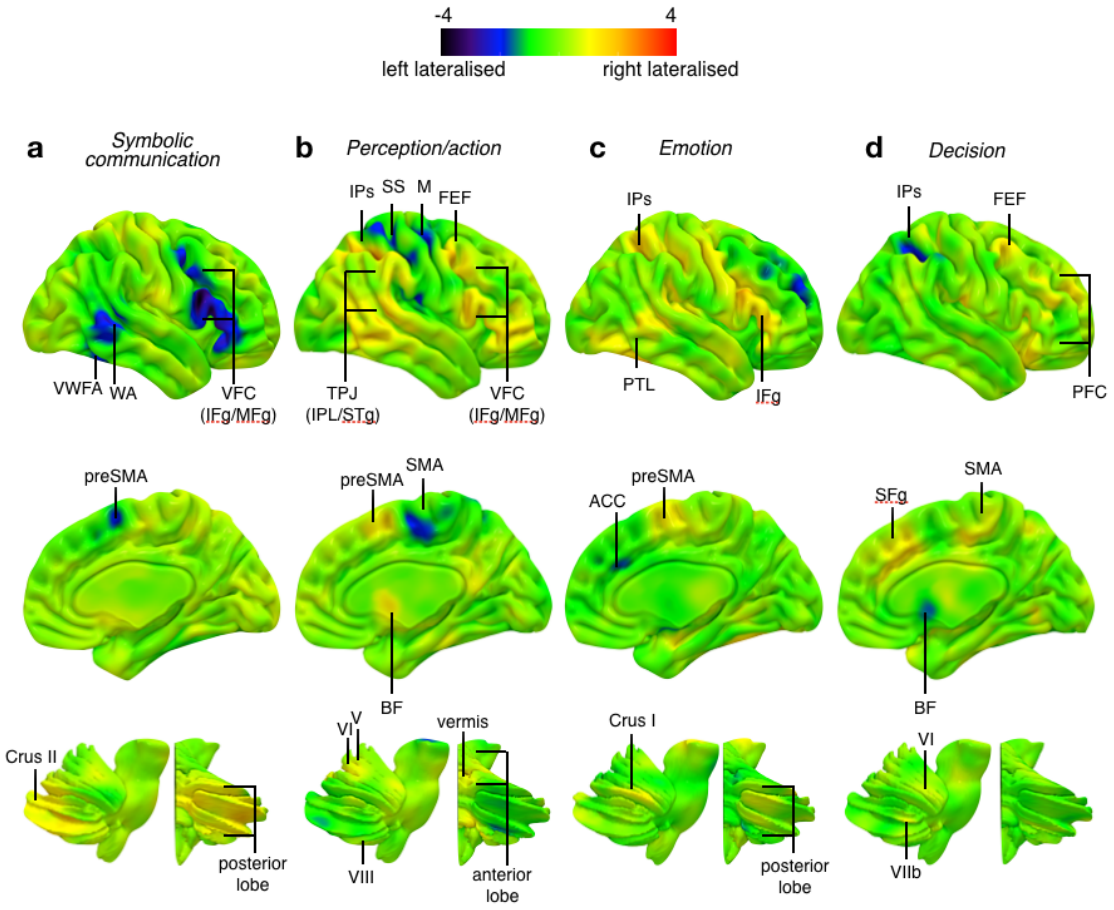

Figure 2. Archetype maps corresponding to the symbolic communication (a) perception/action (b) emotion (c) and decision (d) axes. Upper panel corresponds to the lateral

bioRxiv preprint doi: https://doi.org/10.1101/372300; this version posted December 8, 2018. The copyright holder for this preprint (which was not certified by peer review) is the author/funder, who has granted bioRxiv a license to display the preprint in perpetuity. It is made available under aCC-BY 4.0 International license.

view, middle panel to the medial view and lower panel to the cerebellum view (lateral and posterior views) of the reconstructed pattern of activations. VWFA, visual word form area; WA, Wernicke area; VFC, ventral frontal cortex; IFg, inferior frontal gyrus; MFg, middle frontal gyrus; TPJ, temporo-parietal junction; IPL, inferior parietal lobule; STg, superior temporal gyrus; IPs, intraparietal sulcus; SS, somatosensory cortex; M, motor cortex; FEF, frontal eye field; PTL, posterior temporal lobe; PFC, prefrontal cortex; SMA, supplementary motor area; preSMA, presupplementary motor area; somatosensory cortex, ACC, anterior cingulate cortex; BF, basal forebrain.

Corpus Callosum and functional lateralisation

Given that the microscopic diffusion of water molecules in the brain is easier along rather than across axons, tractography derived from diffusion-weighted magnetic resonance imaging allows for peering into the structural organisation of brain connectivity (**Figure 3a**).

In the following, we analysed the relationship between functional lateralisation and corpus callosum connectivity measures by contrasting the connectivity profiles of lateralised and non-lateralised regions (see Methods for the definition of non-lateralised regions). Two measures of connectivity were employed, both computed by averaging across participants in the HCP sample. The first measure, axonal water fraction [30], is microscopic and is estimated in the midsection of the corpus callosum crossed by streamlines originating from voxels of a selected cortical region. The second measure is macroscopic and estimates the replicability of connections [31, 32] calculated as the proportion of participants in which a voxel is connected to the corpus callosum, which we will refer to as probability of connection for shortness.

By sampling voxels from lateralised and non-lateralised regions, in each hemisphere separately, we first constructed the distribution of the differences in the axonal water fraction between lateralised and non-lateralised regions. **Figure 3b** indicates that the axonal water fraction was consistently lower for corpus callosum voxels projecting onto lateralised regions when compared to non-lateralised voxels. Additionally, the plots suggested a slightly lower axonal water fraction for left hemisphere regions as compared to the right hemisphere.

Next, we constructed an analogous distribution for the probability of connection. **Figure 3c** demonstrates that lateralised regions when compared to non-lateralised voxels did not differ in this macrostructural measure of connectivity.

The previous analysis failed to reveal a categorical difference between lateralised and non-lateralised regions in macroscopic measure of connectivity. However, the degree of functional

bioRxiv preprint doi: https://doi.org/10.1101/372300; this version posted December 8, 2018. The copyright holder for this preprint (which was not certified by peer review) is the author/funder, who has granted bioRxiv a license to display the preprint in perpetuity. It is made available under aCC-BY 4.0 International license.

hemispheric dominance (see Methods section for the definition of this measure) can vary — from a unilateral to a relatively asymmetric pattern of activity. In the latter case, both hemispheres are involved in a function, but one is more active than the other. Therefore, we explored whether a proportional relationship existed between the degree of functional lateralisation and the probability of corpus callosum connectivity.

Figure 3d indicates a negative relationship between the probability of connection and the degree of functional lateralisation, for both the left and the right hemispheres (r = –.81 and r = –.69, respectively, p < .001). As the overall level of activation of two homotopic areas in the left and the right hemispheres may have an influence on its corpus callosum connections, we duplicated the same analysis after regressing out the left and right hemispheres average level of activity for every functionally lateralised voxel. The relationship between the level of functional dominance and the probability of connection to corpus callosum remained unchanged for the left hemisphere (r= –.79) and increased for the right hemisphere (r= –.85).

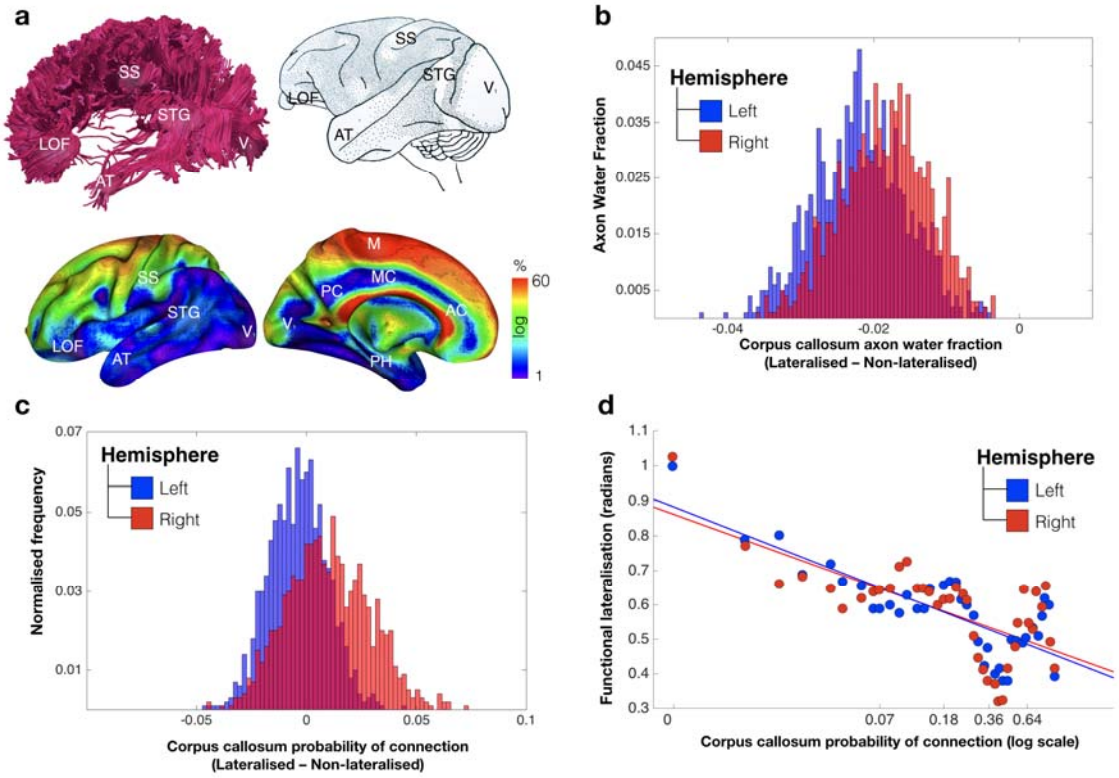

Figure 3. Lateralisation and inter-hemispheric connectivity (**a**) Tractography of the corpus callosum in a representative subject of our study (top left); cortical projection of the corpus callosum derived from axonal tracing in monkeys [33] (top right); cortical projections of the corpus callosum derived from tractography in the participants of our study (bottom). (**b**)

bioRxiv preprint doi: https://doi.org/10.1101/372300; this version posted December 8, 2018. The copyright holder for this preprint (which was not certified by peer review) is the author/funder, who has granted bioRxiv a license to display the preprint in perpetuity. It is made available under aCC-BY 4.0 International license.

Histogram of the difference between lateralised and non-lateralised regions in the corpus callosum axonal water fraction, averaged across participants. (**c**) Histogram of the difference between lateralised and non-lateralised regions in the corpus callosum probability of connection. The measure was calculated as the proportion of participants in which a connection exists between brain's voxels and corpus callosum to the overall HCP sample size. (**d**) Dimensional relationship between the degree of functional lateralisation and the corpus callosum probability of connectivity. LOF, lateral orbitofrontal cortex; SS, somatosensory cortex; STG, superior temporal gyrus; AT, anterior temporal; V1, primary visual area; M, primary motor area; PC, posterior cingulate gyrus; MC, middle cingulate gyrus; AC, anterior cingulate gyrus; PH, parahippocampal gyrus.

Additional supplementary analyses indicated that there was no relationship between the difference in corpus callosum connectivity of lateralised and non-lateralised voxels and their distance from the mid-section of the corpus callosum (**Supplementary Figure 3**).

Discussion

In the present study, we provide for the first time a comprehensive mapping of the functional brain architecture of lateralized cognitive functions. The lateralisation of brain functions had a low-dimensional structure distributed along four functional axes: symbolic communication, perception/action, emotion, and decision-making. Additionally, lateralised regions, as compared to non-lateralised regions, were connected to regions of the corpus callosum with reduced microstructural connectivity. Finally, within the pool of lateralised regions, corpus callosum macrostructural connectivity was proportionally associated to the degree of hemispheric functional dominance.

The meta-analysis of task-related activation maps in relation to cognitive terms replicated several known functional lateralisation profiles (**Figure 1 and 2**). For instance, the term /language/ was associated with dominant responses in prefrontal, superior temporal regions, and inferior parietal regions of the left hemisphere [34]. In association with terms such as /eye movements/stop signal/ we found several regions of right dorsal fronto-parietal and ventral frontal cortex that matched core regions of the dorsal and ventral attention network [26, 35, 36] involved in visuospatial and response inhibition processes. Surprisingly, the term /attention/, possibly not specific enough, was not associated with a specific lateralised component.

bioRxiv preprint doi: https://doi.org/10.1101/372300; this version posted December 8, 2018. The copyright holder for this preprint (which was not certified by peer review) is the author/funder, who has granted bioRxiv a license to display the preprint in perpetuity. It is made available under aCC-BY 4.0 International license.

However, it did show a strong negative weighting on the language component, corroborating previous reports of a balance between language and attention in similar brain regions [37]. Lateralised maps in left and right cortex had counterparts in the contralateral cerebellum in agreement with a role of the cerebellum in supporting cognition [38, 39], and the known anatomical organization of cortico-pontine-cerebellar-thalamic pathways [40]. Even the phylogenetical organisation of functional regions in cerebellar networks was respected [41]. For instance, area Crus II, part of the neo-cerebellum, connected with frontal regions involved in language, showed a significant right lateralisation for the language component. Similarly, Areas V/VI and VIIIb, an anterior superior part of the paleocerebellum connected with sensorimotor cortical regions, showed significant right lateralisation for movement and finger components. These findings support the validity and the anatomical precision of the functional lateralisation maps based on fMRI meta-analyses (also see for comparison our meta-analytic results with a task-based fMRI results on finger tapping in **Supplementary Figure 4**).

The overall functional lateralisation of the brain could be summarized with a low dimensional architecture defined by spatial patterns of activity and groups of cognitive terms. This architecture defined four axes corresponding to symbolic communication, perception/action, emotion, and decision making (**Figure 1**). The association of different terms along the different axis defined domains of function that are not trivially associated. For instance, the axis 'symbolic communication' includes not only left lateralised maps related to the term /language/, but also left and right lateralized parietal maps related to /calculation/ in agreement with recent neuropsychology [42]. The axis perception/action includes left hemisphere component related to motor planning, consistent with the effects of left lesions on motor planning (apraxia) [43, 44], but also right hemisphere maps related to visuospatial attention and response inhibition. As recently shown, attention and motor deficits co-vary after focal lesions [45]. The emotion axis include right hemisphere biased maps for terms such as /expression/fearful/social interactions/, but left hemisphere foci for /autobiographical memory/.

The triangular organisation of this morphospace may be significant in relation to the theory of Pareto optimality. In evolutionary biology [29], the theory posits that in complex systems (e.g. animal morphology [29, 46], animal behaviour [47], cancer [48], ammonite shells [49], bacterial and single gene expression [50, 51], biological circuits [46], structure of polymorphisms [52], Escherichia coli proteome [53]) evolution forces trade-offs among traits: strength in one trait of high

bioRxiv preprint doi: https://doi.org/10.1101/372300; this version posted December 8, 2018. The copyright holder for this preprint (which was not certified by peer review) is the author/funder, who has granted bioRxiv a license to display the preprint in perpetuity. It is made available under aCC-BY 4.0 International license.

evolutionary significance, e.g. solving well one set of problems is associated with relative weakness on other problems. The trait at the vertices of the triangle represent 'archetypes', that is most specialised traits. Pareto optimality distributions in human cognition and behaviour have been recently reported in association with the ability to inhibit immediate reward for larger delayed rewards, a trait associated with numerous other cognitive, behaviour, health, and socioeconomic variables [54].

The low dimensional structure of lateralised functions is consistent with previous findings that reported a low dimensional structure of functional networks [55] and of cognitive performance in both healthy controls [56, 57] and patients [58]. Accordingly, individual performances or deficits are not task-specific but instead shared across a range of cognitive tasks. For example, in stroke patients, two axes of behavioural deficits, one related to language and the other to attention-motor functions, occur [45]. Our result suggests that, at least in stroke, two supplementary axes of deficits might exist along the emotional [59, 60] and decision-making [61] dimensions and that these dimensions tend to be under-represented by the standard behavioural and cognitive examinations. Additionally, the similarity between the grand-scale organisation of functional lateralisation in healthy controls and behavioural deficits in stroke points to the importance of inter-hemispheric connection for recovery from stroke as shown recently by several studies [62, 63].

The distribution of the probability of connection of the corpus callosum onto the brain surface matched the previous atlases that were derived from inter-hemispheric homotopic functional connectivity analyses [64]. Extra conduction time and energy consumption are required to integrate information across hemispheres. Therefore, the role of inter-hemispheric connectivity for functional lateralisation has long been debated in the literature [65]. The current study presents a comprehensive demonstration that functional lateralisation is linked to a decrease of callosal function [66] (i.e. an inter-hemispheric independence), possibly through the mechanisms of callosal myelination and pruning [67]. The alternative hypothesis that functional lateralization depends on a competition between the hemispheres that inhibits each other via the corpus callosum, hence predicting stronger connectivity in lateralised regions, is not supported. Notably, reduced inter-hemispheric communication may improve processing time of lateralized functions, but it may lead to a decreased capacity to recover after a brain injury. This is an issue that deserves further studies as recent studies indicate a proportional recovery similar for different functions (motor, vision, visuospatial attention, language, memory) [68]

bioRxiv preprint doi: https://doi.org/10.1101/372300; this version posted December 8, 2018. The copyright holder for this preprint (which was not certified by peer review) is the author/funder, who has granted bioRxiv a license to display the preprint in perpetuity. It is made available under aCC-BY 4.0 International license.

It is important to stress that several factors limited the interpretation of the findings. For instance, while the meta-analytic approach has the power to summarise thousands of task-related fMRI findings, it is limited by publication biases which prevent a generalisation of the current findings to all brain functions [69]. Additionally, the experimental paradigms probing brain function may systematically use the same or similar material which may have biased some of the asymmetries reported. For instance, processes such as emotion are frequently assessed using emotional faces that typically involve the right hemisphere more than the left hemisphere [70, 71]. Out of the 300 most relevant studies for the term "emotion" in the Neurosynth database, 36% used face stimuli, 28% visual scenes, 16% language-related material, 4% movies, 4% memories, 2% odour and 10% used other materials such as music, conditioned stimuli or inkblots. This, however, appeared to have had a limited effect on our results, because the maps driving the emotion axis did not involve the face fusiform area that is specialised in face perception [72]. However, we cannot rule out the possibility that biases in label selection by the experimenters that ran the studies housed in neurosynth may in part affect our findings. Another issue concerns whether the left lateralisation of some functions, such as finger tapping, movement and touch, could be related to the laterality of stimulus presentation or response. While we cannot rule out this possibility, lesion studies indicate that apraxia, a deficit of motor planning and control, occurs more frequently and severely after left hemisphere damage [43, 44]. In addition, we found an excellent agreement between the foci of lateralised response in left SMA and left thalamus identified in our meta-analysis, and the results of a finger tapping task in a functional MRI study of 142 right-handed participants that controlled for the laterality of the manual response (**Supplementary Figure 4**). A fourth limitation, which is not specific to the current study, is that *f*MRI signal on the medial wall can be blurred at the acquisition stage, due to voxel size and spatial smoothing applied to the *f*MRI data as a standard (and typically compulsory) pre-processing step. This problem can limit the ability to detect lateralised regions along the medial wall of the brain or in regions close to the midline. Even though we observed several lateralised regions on the medial walls of the brain, it is not possible to estimate how many putatively lateralised regions were lost due to limited spatial resolution. Finally, the limitation of the connectivity analyses derived from diffusion-weighted imaging [73] also prevented us from investigating with confidence the distinct contribution of homotopic and heterotopic areas to the functional lateralisation as well as smaller interhemispheric connections such as the anterior commissure, hippocampal commissure, massa intermedia (i.e. thalamus), tectal commissure of Forel (i.e. tegmentum), habenular commissure and reticular commissure (i.e. brainstem) [74]. The advent of new

bioRxiv preprint doi: https://doi.org/10.1101/372300; this version posted December 8, 2018. The copyright holder for this preprint (which was not certified by peer review) is the author/funder, who has granted bioRxiv a license to display the preprint in perpetuity. It is made available under aCC-BY 4.0 International license.

diffusion imaging methods [75], as well as post-mortem investigations [76], might circumvent this bias in the future.

In conclusion, the present analysis provides us with a comprehensive view of functional lateralisation in humans, which appears to be organized in four domains: symbolic communication, perception/action, emotion-related and decision-making functions. It also reveals some of its mechanisms, such as the relationship between functional lateralisation and the strength of communication between the hemispheres. The similarity between the current findings and recent work on neurological symptoms give rise to new hypotheses on the mechanisms that support brain recovery after a brain lesion.

bioRxiv preprint doi: https://doi.org/10.1101/372300; this version posted December 8, 2018. The copyright holder for this preprint (which was not certified by peer review) is the author/funder, who has granted bioRxiv a license to display the preprint in perpetuity. It is made available under aCC-BY 4.0 International license.

Methods

Code Availability

The code used in the following analyses is available on request to slava.karolis@kcl.ac.uk

Datasets

In this study we used a meta-analytic approach to the functional MRI studies described by Yarkoni et al. ([18]; http ://Neurosynth.org). We downloaded the Neurosynth database that contained 3107 reversed unthresholded functional maps and the details of 11406 literature sources as of the 25th of September 2017.

Structural connectome data were derived from the diffusion-weighted imaging dataset of 163 participants acquired at 7 Tesla by the Human Connectome Project Team [77]. (http://www.humanconnectome.org/study/hcp-young-adult/) (WU-Minn Consortium; Principal investigators: David Van Essen and Kamil Ugurbil; 1U54MH091657). This was funded by the 16 NIH Institutes and Centers that support the NIH Blueprint for Neuroscience Research; and by the McDonnell Center for Systems Neuroscience at Washington University.

Data pre-processing

A) **Neurosynth data**

Two researchers (V.K & M.TdS) acted as judges, selecting terms that, in their view, were related to specific cognitive processes. The selection procedure consisted of two stages. During the first stage, the judges made their selection independently. Brain anatomical (e.g., “salience network"), psychiatric (e.g., “schizophrenia”), and pathological (e.g., “alzheimer”) terms were systematically excluded. The two judges agreed on 422 terms as related to cognitive processes as well as 2309 unrelated terms that were to be discarded (88% reproducibility). For the remaining terms, the judges made their decision together. In the end, 590 cognitive terms were selected for the study.

In the present analysis, we corrected for the anatomical differences between the left and the right hemispheres to focus on the functional asymmetries. Given that the Neurosynth functional maps are provided in the standard 2mm MNI template space, which is not symmetric, we co-registered non-linearly the MNI template to a MNI symmetrical template, available at http://www.bic.mni.mcgill.ca/ServicesAtlases/ICBM152NLin2009, using the Greedy symmetric diffeomorphic normalization (GreedySyN) pipeline distributed with the Advanced Normalization Tools (ANTs, http://stnava.github.io/ANTs/) [78]. The symmetrical

bioRxiv preprint doi: https://doi.org/10.1101/372300; this version posted December 8, 2018. The copyright holder for this preprint (which was not certified by peer review) is the author/funder, who has granted bioRxiv a license to display the preprint in perpetuity. It is made available under aCC-BY 4.0 International license.

template was downsampled to a 2 mm voxel size to match the voxel dimensions of the standard template. The estimated transformation between non-symmetrical and symmetrical MNI spaces were then applied to all functional maps.

The following steps were performed to obtain lateralisation indices for each functional map following their co-registration with the symmetrical template. Firstly, we split the functional maps into the left- and right-hemisphere parts and smoothed the resulting maps using a 6 mm FWHM Gaussian filter. We then flipped the left-hemisphere maps and subtracted them from unflipped right-hemisphere maps in order to obtain laterality indices (LI) maps (see [26] for a similar approach). Positive and negative values in these maps would signify a higher meta-analytic evidence for, respectively, right and left lateralisation of the function associated with a term.

B) **Structural connectome data**

The scanning parameters have previously been described in Vu et al. [77]. In brief, each diffusion-weighted imaging consisted of a total of 132 near-axial slices acquired with an acceleration factor of 3 [79], isotropic (1.05 mm3) resolution and coverage of the whole head with a TE of 71.2 ms and with a TR of 7000 ms. At each slice location, diffusion-weighted images were acquired with 65 uniformly distributed gradients in multiple Q-space shells [80] and 6 images with no diffusion gradient applied. This acquisition was repeated 4 times with a b-value of 1000 and 2000 $s.mm^{-2}$ in pairs with left-to-right and right-to-left phase-encoding directions. The default HCP preprocessing pipeline (v3.19.0) was applied to the data [81, 82]. In short, the susceptibility-induced off-resonance field was estimated from pairs of images with diffusion gradient applied with distortions going in opposite directions [83] and corrected for the whole diffusion-weighted dataset using TOPUP [84]. Subsequently, motion and geometrical distortion were corrected using the EDDY tool as implemented in FSL.

ExploreDTI toolbox for Matlab (http://www.exploredti.com [85, 86]) has been used to extract estimates of axonal water fraction [30]. Next, we discarded the volumes with a b-value of 1000 $s.mm^{-2}$ and whole-brain deterministic tractography was subsequently performed in the native DWI space using StarTrack software (https://www.mr-startrack.com). A damped Richardson-Lucy algorithm was applied for spherical deconvolutions [87]. A fixed fibre response corresponding to a shape factor of α = 1.5x10-3 mm2/s was adopted, coupled with the

bioRxiv preprint doi: https://doi.org/10.1101/372300; this version posted December 8, 2018. The copyright holder for this preprint (which was not certified by peer review) is the author/funder, who has granted bioRxiv a license to display the preprint in perpetuity. It is made available under aCC-BY 4.0 International license.

geometric damping parameter of 8. Two hundred algorithm iterations were run. The absolute threshold was defined as 3 times the spherical fibre orientation distribution (FOD) of a grey matter isotropic voxel and the relative threshold as 8% of the maximum amplitude of the FOD [88]. A modified Euler algorithm [89] was used to perform the whole brain streamline tractography, with an angle threshold of 35°, a step size of 0.5 mm, and a minimum streamline length of 15mm.

We co-registered the structural connectome data to the standard MNI 2mm space using the following steps: First, whole brain streamline tractography was converted into streamline density volumes where the intensities corresponded to the number of streamlines crossing each voxel. Second, a study-specific template of streamline density volumes was generated using the Greedy symmetric diffeomorphic normalisation (GreedySyN) pipeline distributed with ANTs. This provided an average template of the streamline density volumes for all subjects. The template was then co-registered with a standard 2mm MNI152 template using flirt tool implemented in FSL. This step produced a streamline density template in the MNI152 space. Third, individual streamline density volumes were registered to the streamline density template in the MNI152 space template and the same transformation was applied to the individual whole brain streamline tractography using the trackmath tool distributed with the software package Tract Querier [90], and to the axonal water fraction maps, using ANTs GreedySyn. This step produced a whole brain streamline tractography and axonal water fraction maps in the standard MNI152 space.

Statistical analyses of laterality (see Supplementary Figure 5)

A) Determination of functionally lateralised regions

In these analyses, completed in two steps, we thought to identify the regions with significant functional lateralisation. In the first step, we addressed the redundancy while preserving the richness of the Neurosynth data. For instance, many selected terms were related as singular and plural forms of the same word (e.g, “visual form” and “visual forms”) and therefore their maps are likely to be very similar. To this end, we reduced the dimensionality of the data using a data-driven varimax-rotated principal component (PC) analysis implemented in SPSS (SPSS, Chicago, IL) with the LI maps as inputs [91, 92, 93]. Following a standard principal component analysis, involving the eigendecomposition of the covariance matrix, 171 extracted orthogonal components with eigenvalues more than the grand average were

bioRxiv preprint doi: https://doi.org/10.1101/372300; this version posted December 8, 2018. The copyright holder for this preprint (which was not certified by peer review) is the author/funder, who has granted bioRxiv a license to display the preprint in perpetuity. It is made available under aCC-BY 4.0 International license.

submitted to the varimax-rotation procedure using Kaiser normalisation criterion [94], with a maximum of 1000 iterations for convergence. This accounted for 72.6% of variance in the data. The distribution of loadings along varimax-rotated principal components is typically skewed and only a few items receive large loadings. Subsequently, for the purpose of discussing the results, components were labelled according to the term(s) with the largest loadings (**Supplementary Table 3)**.

In the second step, general linear modelling was employed to identify voxels with a significant lateralisation associated with a particular component. In this analysis, the principal components were used as a set of predictors to fit the LI maps and obtain beta maps, i.e., component spatial maps. The permutation test was performed to identify significantly lateralised regions. Given that varimax rotation may impose some correlations between the columns of the principal component matrix, we performed permutations on the rows of the unrotated matrix, subsequently applying component rotation and calculating a random map on each permutation in the same way as it was done for the real principal components. This procedure allowed us to mimic the correlational structure of the unpermuted data and provide a more robust test of significance. In order to account for multiple comparisons, the maximal statistics approach was used whereby the spatial map values for the real principal components were compared to the maximal a (either positively or negatively) value across a whole random map on each permutation. 5000 permutations were run. The voxels were considered as showing a significant lateralisation if they simultaneously satisfied two criteria: 1) their spatial map values were in 97.5% cases higher or lower than, respectively, maximal positive and negative the values obtained via permutations (i.e., $p < .05$, two-tailed and FWE-corrected); 2) they formed a cluster of at least 20 voxels. The second criterion was used to exclude small and possibly spurious effects observed in a small number of voxels.

B) **Multivariate embedding**

In order to characterise a low-dimensional structure of functional brain lateralisation, a spectral embedding of the LI maps was performed using eigen decomposition of graph normalised Laplacian of similarity matrix [95]. The method sought to uncover geometric features in the similarities between the lateralisation maps by converting these similarities into distances between lateralisation maps in the embedded space (the higher similarity between lateralisation profiles, the smaller the distance). Here we concentrated only on the variances which were accounted for by the 171 components analysed in the present study. To this end,

bioRxiv preprint doi: https://doi.org/10.1101/372300; this version posted December 8, 2018. The copyright holder for this preprint (which was not certified by peer review) is the author/funder, who has granted bioRxiv a license to display the preprint in perpetuity. It is made available under aCC-BY 4.0 International license.

the LI maps were "de-noised," in a sense that they were reconstructed as the matrix product of 171 components and their spatial maps. Every element of the similarity matrix was calculated as a dot product taken for a pair of "denoised" LI maps across all voxels (i.e., an element of the similarity matrix was a sum of products of voxelwise values for a pair of maps). Negative values were zeroed to permit estimability. The embedding dimensions were ordered according to their eigenvalues, from small to large. The first non-informative dimension associated with a zero eigenvalue was dropped. In the analysis we sought to determine whether there exists a structure in a low dimensional representation of the data, specifically data structural triangularity, and if it does, in how many dimensions this structure is preserved (for eigenvalue plot - see **Supplementary Figure 6**). The triangular structure was quantified as a t-ratio, i.e., a ratio between the area of the convex hull encompassing all points in embedded space and an encompassing triangle of a minimal area [29]. These values were compared to the t-ratios of random LI maps. These random maps were obtained by generating 2000 sets of 590 random maps via the permutation of the voxel order. For each set, random LI maps were calculated for each pair and then submitted to varimax analysis with the number of principal components = 171. The embedding procedure was identical to the procedure applied to non-random LI maps. The dimensional span of triangular organisation was evaluated by testing if t-ratio for non-random LI maps was greater than t-ratios of random LI maps in each 2-dimensional subspace of embedding ($p < .05$, Bonferroni-corrected). The label for the axes was defined ad-hoc according to one or a few terms situated at the vertices of the triangle. Archetype maps were approximated using multiple regression approach. We first regressed the values in each voxel across the "denoised" LI maps onto corresponding maps' coordinates in the first 171 dimensions of the embedded space (i.e., matching the number of components used for "denoising"). This provided an estimated contribution of each embedded dimension to the lateralisation index. We then obtained the archetype maps by evaluating regression coefficients for the dimensions where the triangular structure was observed at the estimated locations of the archetypes (i.e., at the vertices of "simplex" - multidimensional triangular).

Analyses of function-structure relationship (see Supplementary Figure 7)

A) Determination of non-lateralised regions

In the following analyses we contrasted the connectivity profiles of lateralised regions with regions that do not show a significant lateralisation but nevertheless show a significant involvement at least in one function. The latter was identified by repeating the analyses

bioRxiv preprint doi: https://doi.org/10.1101/372300; this version posted December 8, 2018. The copyright holder for this preprint (which was not certified by peer review) is the author/funder, who has granted bioRxiv a license to display the preprint in perpetuity. It is made available under aCC-BY 4.0 International license.

outlined in the section "Determination of functionally lateralised regions" with the original Neurosynth functional maps as inputs. This rendered 69 components, accounting for 70.6% of variance. For closer comparability, the analysis was run in the symmetrical space and for the left and right hemispheres separately. The voxels were considered to have no significant lateralisation if they met the following criteria: 1) passed the significance threshold for at least one component and one hemisphere; 2) were non-overlapping with lateralised voxels; and 3) were homologues of the voxels meeting criteria 1) and 2) in the opposite hemisphere. A shortcut term "non-lateralised" regions was used to denominate voxels without significant lateralisation in the remaining text. This provides a conservative contrast for the lateralised regions because, by virtue of the frequentist statistical approach, the non-lateralised regions would also include voxels demonstrating a considerable lateralisation but failing to meet the statistical criteria of significance used in the study. The number of non-lateralised voxels was 3.6 times greater than the number of lateralised voxels.

B) **Measures of the connectivity strength**

The following steps were used for structure-function relationships. First, we combined the spatial maps of significantly lateralised voxels, irrespective of the left and right polarity of lateralisation. Second, we transformed the combined map back into the regular MNI space for a joint analysis with diffusion information using an inverse of the MNI non-symmetrical to MNI symmetrical template deformations estimated above. Finally, we projected the combined map onto the white matter boundary of the non-symmetrical MNI template in each hemisphere and subsequently selected tractography from these voxels to the corpus callosum. The same procedures were applied to the maps of non-lateralised regions.

Two measures for the strength of structural inter-hemispheric connectivity were analysed. The first, microstructural, measure referred to the axonal water fraction, averaged across participants in the HCP sample, in the voxels of corpus callosum which were hit by streamlines from selected lateralised (or non-lateralised) regions. The second, macrostructural, measure of connectivity, was defined in terms of connection replicability [32] between brain's voxels and corpus callosum, i.e., as a proportion of participants in which a connection exists between brain's voxels and corpus callosum to the overall HCP sample size. We will refer to this measure as a "probability of connection" for shortness.

C) **Comparison of the connectivity between lateralised and non-lateralised regions**

bioRxiv preprint doi: https://doi.org/10.1101/372300; this version posted December 8, 2018. The copyright holder for this preprint (which was not certified by peer review) is the author/funder, who has granted bioRxiv a license to display the preprint in perpetuity. It is made available under aCC-BY 4.0 International license.

The comparison of connectivity between lateralised and non-lateralised regions was performed by sampling subsets of voxels (without replacement) from the pools of lateralised and non-lateralised cortical voxels. A sample from each pool was equal to 5% of the entire number of voxels in that pool (i.e., ensuring that the within-pool spatial frequency of drawn samples was equal between pools). For each subset we calculated an average value for probability of connection and a weighted average for callosal axonal water fraction, where a weight for a voxel was given as a connection replicability between this voxel and any voxel in a sampled subset. A negative value would indicate a weaker connectivity of the lateralised voxels. The distributions of the difference in the connectivity measures between lateralised and non-lateralised cortical regions were obtained by repeating the procedure 1000 times and for each hemisphere separately.

D) **Hemispheric dominance**

The degree of functional hemispheric dominance was evaluated in radians as an arctangent of the ratio between the strengths of activation in two hemispheres. Pi/4 was subtracted from this value to ensure that the absolute magnitude of this value increases if the task activation is unilateral and decreases if both hemispheres demonstrate comparable levels of task activity. Given that a partial spatial overlap between lateralised regions associated with different components is possible, in the analyses we picked the dominance values associated with components that rendered the largest z-score in a particular voxel. In order to obtain robust estimate for the relationship between hemispheric dominance and the strength of inter-hemispheric connectivity, the voxels were binned by the probabilities of connection such that the smallest bin width was of the size equal to 1/163 and increased with the probability of connection (given by logspace function in Matlab). This procedure was used to partially compensate for the fact that only a very limited number of voxels had a high probability of connection to the corpus callosum, whereas the majority were characterised by small values. We also estimated the voxel's average activity between left and right hemispheres (i.e., (left + right hemisphere activity) / 2) and used it as a covariate of non-interest in the analyses looking at the relationship between hemispheric dominance and other measures.

Authors contribution

V.K. implemented the methods, performed the analyses and wrote the manuscript. M.C. conceived and coordinated the study, and wrote the manuscript. M.T.S. conceived and coordinated the study, reviewed the neuroimaging data, wrote the manuscript, and provided

bioRxiv preprint doi: https://doi.org/10.1101/372300; this version posted December 8, 2018. The copyright holder for this preprint (which was not certified by peer review) is the author/funder, who has granted bioRxiv a license to display the preprint in perpetuity. It is made available under aCC-BY 4.0 International license.

funding.

Acknowledgments

We particularly thank Nathalie Tzourio-Mazoyer and her team (GIN) for useful discussion and for providing us with fMRI maps of left and right hands finger tapping. We also thank Lauren Sakuma for useful discussion and edits to the manuscript. The research leading to these results received funding from the "Agence Nationale de la Recherche" [grant number ANR-13- JSV4-0001-01] and the European Research Council (ERC) Consolidator Grant "DISCONNECTOME" [ERC-2018-COG 818521]. Additional financial support comes from the program "Investissements d'avenir" ANR-10-IAIHU-06 and the Fondation pour la Recherche Medicale [grant number DEQ20150331725]. M.C. was supported by NIH R01NS095741, and a strategic grant from the University of Padua. MC was a visiting professor at the Institut du Cerveau and Moelle Epiniere (ICM) in Paris where the research was conducted.

Data Availability

The dataset analysed during the current study are available at https://www.humanconnectome.org and http://www.Neurosynth.org.

In addition, processed data are available on request to the corresponding authors michel.thiebaut@gmail.com and slava.karolis@kcl.ac.uk.

References

1. Geschwind N, Galaburda AM. Cerebral lateralization. Biological mechanisms, associations, and pathology: I. A hypothesis and a program for research. *Arch Neurol* **42**, 428-459 (1985).

2. Sperry RW. *Lateral Specialization in the Surgically Separated Hemispheres*. Rockefeller University Press (1974).

3. Kong XZ, *et al.* Mapping cortical brain asymmetry in 17,141 healthy individuals worldwide via the ENIGMA Consortium. *Proc Natl Acad Sci U S A* **115**, E5154-E5163 (2018).

4. Toga AW, Thompson PM. Mapping brain asymmetry. *Nat Rev Neurosci* **4**, 37-48 (2003).

5. Herve PY, Zago L, Petit L, Mazoyer B, Tzourio-Mazoyer N. Revisiting human hemispheric specialization with neuroimaging. *Trends Cogn Sci* **17**, 69-80 (2013).

bioRxiv preprint doi: https://doi.org/10.1101/372300; this version posted December 8, 2018. The copyright holder for this preprint (which was not certified by peer review) is the author/funder, who has granted bioRxiv a license to display the preprint in perpetuity. It is made available under aCC-BY 4.0 International license.

6. Wexler BE. Cerebral laterality and psychiatry: a review of the literature. *Am J Psychiatry* **137**, 279-291 (1980).

7. Bishop DV. Cerebral asymmetry and language development: cause, correlate, or consequence? *Science* **340**, 1230531 (2013).

8. Bartolomeo P, Thiebaut de Schotten M. Let thy left brain know what thy right brain doeth: Inter-hemispheric compensation of functional deficits after brain damage. *Neuropsychologia*, (2016).

9. Forkel SJ, *et al.* Anatomical predictors of aphasia recovery: a tractography study of bilateral perisylvian language networks. *Brain* **137**, 2027-2039 (2014).

10. Lunven M, *et al.* White matter lesional predictors of chronic visual neglect: a longitudinal study. *Brain* **138**, 746-760 (2015).

11. Siegel JS, *et al.* Disruptions of network connectivity predict impairment in multiple behavioral domains after stroke. *Proc Natl Acad Sci U S A* **113**, E4367-4376 (2016).

12. Hopkins WD, Cantalupo C. Theoretical Speculations on the Evolutionary Origins of Hemispheric Specialization. *Current Directions in Psychological Science* **17**, 233-237 (2008).

13. Tzourio-Mazoyer N. *Intra- and Inter-hemispheric Connectivity Supporting Hemispheric Specialization*. Springer (2016).

14. Ringo JL, Doty RW, Demeter S, Simard PY. Time is of the essence: a conjecture that hemispheric specialization arises from interhemispheric conduction delay. *Cereb Cortex* **4**, 331-343 (1994).

15. Markov NT, Ercsey-Ravasz M, Van Essen DC, Knoblauch K, Toroczkai Z, Kennedy H. Cortical high-density counterstream architectures. *Science* **342**, 1238406 (2013).

16. Jäncke L, Steinmetz H. Brain size: a possible source of interindividual variability in corpus callosum morphology. In: *Brain size: a possible source of interindividual variability in corpus callosum morphology* (ed^(eds Zaidel E IM, Pascual-Leone A). Plenum Press (1998).

17. Josse G, Seghier ML, Kherif F, Price CJ. Explaining function with anatomy: language lateralization and corpus callosum size. *J Neurosci* **28**, 14132-14139 (2008).

18. Yarkoni T, Poldrack RA, Nichols TE, Van Essen DC, Wager TD. Large-scale automated synthesis of human functional neuroimaging data. *Nat Methods* **8**, 665-670 (2011).

19. Van Essen DC, *et al.* The WU-Minn Human Connectome Project: an overview. *Neuroimage* **80**, 62-79 (2013).

bioRxiv preprint doi: https://doi.org/10.1101/372300; this version posted December 8, 2018. The copyright holder for this preprint (which was not certified by peer review) is the author/funder, who has granted bioRxiv a license to display the preprint in perpetuity. It is made available under aCC-BY 4.0 International license.

20. Yakovlev PJ, Rakic P. Pattern of decussation of bulbar pyramids and distribution of pyramidal tracts on two sides of the spinal cord. *Trans Amer Neurol Assoc* **91**, 366-367 (1966).

21. Geschwind N, Levitsky W. Human brain: left-right asymmetries in temporal speech region. *Science* **161**, 186-187 (1968).

22. Amunts K, *et al.* Asymmetry in the human motor cortex and handedness. *Neuroimage* **4**, 216-222 (1996).

23. Yousry TA, *et al.* Localization of the motor hand area to a knob on the precentral gyrus. A new landmark. *Brain* **120 (Pt 1)**, 141-157 (1997).

24. Byblow WD, Chua R, Goodman D. Asymmetries in Coupling Dynamics of Perception and Action. *J Mot Behav* **27**, 123-137 (1995).

25. Berlucchi G, Heron W, Hyman R, Rizzolatti G, Umiltà C. Simple reaction time of ipsilateral and contralateral hand to lateralized visual stimuli. *Brain* **94**, 419-430 (1971).

26. Shulman GL, Pope DL, Astafiev SV, McAvoy MP, Snyder AZ, Corbetta M. Right hemisphere dominance during spatial selective attention and target detection occurs outside the dorsal frontoparietal network. *Journal of Neuroscience* **30**, 3640-3651 (2010).

27. Luo B, Wilson RC, Hancock ER. Spectral embedding of graphs. *Pattern Recognition* **36**, 2213-2230 (2003).

28. Barthélemy M. Spatial networks. *Physics Reports* **499**, 1-101 (2011).

29. Shoval O, *et al.* Evolutionary trade-offs, Pareto optimality, and the geometry of phenotype space. *Science* **336**, 1157-1160 (2012).

30. Fieremans E, Jensen JH, Helpern JA. White matter characterization with diffusional kurtosis imaging. *Neuroimage* **58**, 177-188 (2011).

31. Thiebaut de Schotten M, *et al.* Atlasing location, asymmetry and inter-subject variability of white matter tracts in the human brain with MR diffusion tractography. *Neuroimage* **54**, 49-59 (2011).

32. Karolis VR, *et al.* Reinforcement of the Brain's Rich-Club Architecture Following Early Neurodevelopmental Disruption Caused by Very Preterm Birth. *Cereb Cortex* **26**, 1322-1335 (2016).

33. Myers RE. Organization of forebrain commissures. In: *Functions of the Corpus Callosum* (ed^(eds Ettlinger EG). CIBA Foundation Study Group 20 (1965).

34. Mazoyer B, *et al.* Gaussian mixture modeling of hemispheric lateralization for language in a large sample of healthy individuals balanced for handedness. *PLoS One* **9**, e101165 (2014).

bioRxiv preprint doi: https://doi.org/10.1101/372300; this version posted December 8, 2018. The copyright holder for this preprint (which was not certified by peer review) is the author/funder, who has granted bioRxiv a license to display the preprint in perpetuity. It is made available under aCC-BY 4.0 International license.

35. Corbetta M, Shulman GL. Control of goal-directed and stimulus-driven attention in the brain. *Nature Reviews Neuroscience* **3**, 201-215 (2002).

36. Thiebaut de Schotten M, *et al.* A lateralized brain network for visuospatial attention. *Nat Neurosci* **14**, 1245-1246 (2011).

37. Zago L, *et al.* The association between hemispheric specialization for language production and for spatial attention depends on left-hand preference strength. *Neuropsychologia* **93**, 394-406 (2016).

38. Schmahmann JD. An emerging concept. The cerebellar contribution to higher function. *Arch Neurol* **48**, 1178-1187 (1991).

39. Schmahmann JD, Caplan D. Cognition, emotion and the cerebellum. *Brain* **129**, 290-292 (2006).

40. Schmahmann JD. The Cerebrocerebellar System. In: *Essentials of Cerebellum and Cerebellar Disorders: A Primer For Graduate Students* (ed^(eds Gruol DL, Koibuchi, N., Manto, M., Molinari, M., Schmahmann, J.D., Shen, Y.). Springer International Publishing (2016).

41. Buckner RL, Krienen FM. The evolution of distributed association networks in the human brain. *Trends Cogn Sci* **17**, 648-665 (2013).

42. Semenza C, Benavides-Varela S. Reassessing lateralization in calculation. *Philos Trans R Soc Lond B Biol Sci* **373**, (2017).

43. Della Sala S, Faglioni P, Motto C, Spinnler H. Hemisphere asymmetry for imitation of hand and finger movements, Goldenberg's hypothesis reworked. *Neuropsychologia* **44**, 1496-1500 (2006).

44. Goldenberg G. Apraxia and beyond: life and work of Hugo Liepmann. *Cortex* **39**, 509-524 (2003).

45. Corbetta M, *et al.* Common behavioral clusters and subcortical anatomy in stroke. *Neuron* **85**, 927-941 (2015).

46. Szekely P, Korem Y, Moran U, Mayo A, Alon U. The Mass-Longevity Triangle: Pareto Optimality and the Geometry of Life-History Trait Space. *PLoS Comput Biol* **11**, e1004524 (2015).

47. Gallagher T, Bjorness T, Greene R, You YJ, Avery L. The geometry of locomotive behavioral states in C. elegans. *PLoS One* **8**, e59865 (2013).

48. Hart Y, *et al.* Inferring biological tasks using Pareto analysis of high-dimensional data. *Nature Methods* **12**, 233–235 (2015).

49. Tendler A, Mayo A, Alon U. Evolutionary tradeoffs, Pareto optimality and the morphology of ammonite shells. *BMC Syst Biol* **9**, 12 (2015).

bioRxiv preprint doi: https://doi.org/10.1101/372300; this version posted December 8, 2018. The copyright holder for this preprint (which was not certified by peer review) is the author/funder, who has granted bioRxiv a license to display the preprint in perpetuity. It is made available under aCC-BY 4.0 International license.

50. Thogersen JC, Morup M, Damkiaer S, Molin S, Jelsbak L. Archetypal analysis of diverse Pseudomonas aeruginosa transcriptomes reveals adaptation in cystic fibrosis airways. *BMC Bioinformatics* **14**, 279 (2013).

51. Korem Y, *et al*. Geometry of the Gene Expression Space of Individual Cells. *PLoS Comput Biol* **11**, e1004224 (2015).

52. Sheftel H, Szekely P, Mayo A, Sella G, Alon U. Evolutionary trade-offs and the structure of polymorphisms. *Philos Trans R Soc Lond B Biol Sci* **373**, (2018).

53. Kocillari L, Fariselli P, Trovato A, Seno F, Maritan A. Signature of Pareto optimization in the Escherichia coli proteome. *Sci Rep* **8**, 9141 (2018).

54. Cona G, Kocillari L, Palombit A, Bertoldo A, Maritan A, Corbetta M. Archetypes of human cognition defined by time preference for reward and their brain correlates: An evolutionary trade-off approach. *Neuroimage* **185**, 322-334 (2018).

55. Liu H, Stufflebeam SM, Sepulcre J, Hedden T, Buckner RL. Evidence from intrinsic activity that asymmetry of the human brain is controlled by multiple factors. *Proc Natl Acad Sci U S A* **106**, 20499-20503 (2009).

56. Friedman NP, Miyake A. Unity and diversity of executive functions: Individual differences as a window on cognitive structure. *Cortex*, (2016).

57. Cona GF, Kocillari L, Palombit A, Bertoldo A, Maritan A, Corbetta M. Archetypes in human behavior and their brain correlates: An evolutionary trade-off approach. *bioRxiv*, (2018).

58. Corbetta M, Siegel JS, Shulman GL. On the low dimensionality of behavioral deficits and alterations of brain network connectivity after focal injury. *Cortex*, (2018).

59. Tzourio-Mazoyer N, Joliot M, Marie D, Mazoyer B. Variation in homotopic areas' activity and inter-hemispheric intrinsic connectivity with type of language lateralization: an FMRI study of covert sentence generation in 297 healthy volunteers. *Brain Struct Funct*, (2015).

60. Ghika-Schmid F, van Melle G, Guex P, Bogousslavsky J. Subjective experience and behavior in acute stroke: the Lausanne Emotion in Acute Stroke Study. *Neurology* **52**, 22-28 (1999).

61. Azuar C, *et al*. Testing the model of caudo-rostral organization of cognitive control in the human with frontal lesions. *Neuroimage* **84**, 1053-1060 (2014).

62. Siegel JS, *et al*. Re-emergence of modular brain networks in stroke recovery. *Cortex* **101**, 44-59 (2018).

63. Ramsey LE, *et al.* Normalization of network connectivity in hemispatial neglect recovery. *Ann Neurol* **80**, 127-141 (2016).

bioRxiv preprint doi: https://doi.org/10.1101/372300; this version posted December 8, 2018. The copyright holder for this preprint (which was not certified by peer review) is the author/funder, who has granted bioRxiv a license to display the preprint in perpetuity. It is made available under aCC-BY 4.0 International license.

64. Joliot M, *et al.* AICHA: An atlas of intrinsic connectivity of homotopic areas. *J Neurosci Methods* **254**, 46-59 (2015).

65. Tzourio-Mazoyer N, Seghier ML. The neural bases of hemispheric specialization. *Neuropsychologia* **93**, 319-324 (2016).

66. Gazzaniga MS. Cerebral specialization and interhemispheric communication: does the corpus callosum enable the human condition? *Brain* **123 (Pt 7)**, 1293-1326 (2000).

67. Luders E, Thompson PM, Toga AW. The development of the corpus callosum in the healthy human brain. *J Neurosci* **30**, 10985-10990 (2010).

68. Ramsey LE, Siegel JS, Lang CE, Strube M, Shulman GL, Corbetta M. Behavioural clusters and predictors of performance during recovery from stroke. *Nat Hum Behav* **1**, (2017).

69. Jennings RG, Van Horn JD. Publication bias in neuroimaging research: implications for meta-analyses. *Neuroinformatics* **10**, 67-80 (2012).

70. Gazzaniga MS, Smylie CS. Facial recognition and brain asymmetries: clues to underlying mechanisms. *Ann Neurol* **13**, 536-540 (1983).

71. Davidson RJ, Shackman AJ, Maxwell JS. Asymmetries in face and brain related to emotion. *Trends Cogn Sci* **8**, 389-391 (2004).

72. Kanwisher N, McDermott J, Chun MM. The fusiform face area: a module in human extrastriate cortex specialized for face perception. *J Neurosci* **17**, 4302-4311 (1997).

73. Maier-Hein KH, *et al.* The challenge of mapping the human connectome based on diffusion tractography. *Nat Commun* **8**, 1349 (2017).

74. Catani M, Thiebaut de Schotten M. *Atlas of Human Brain Connections*. Oxford University Press (2012).

75. Girard G, *et al.* AxTract: Toward microstructure informed tractography. *Hum Brain Mapp* **38**, 5485-5500 (2017).

76. De Benedictis A, *et al.* New insights in the homotopic and heterotopic connectivity of the frontal portion of the human corpus callosum revealed by microdissection and diffusion tractography. *Hum Brain Mapp* **37**, 4718-4735 (2016).

77. Vu AT, *et al.* High resolution whole brain diffusion imaging at 7T for the Human Connectome Project. *Neuroimage* **122**, 318-331 (2015).

78. Avants BB, Tustison NJ, Song G, Cook PA, Klein A, Gee JC. A reproducible evaluation of ANTs similarity metric performance in brain image registration. *Neuroimage* **54**, 2033-2044 (2011).

bioRxiv preprint doi: https://doi.org/10.1101/372300; this version posted December 8, 2018. The copyright holder for this preprint (which was not certified by peer review) is the author/funder, who has granted bioRxiv a license to display the preprint in perpetuity. It is made available under aCC-BY 4.0 International license.

79. Moeller S, *et al.* Multiband multislice GE-EPI at 7 tesla, with 16-fold acceleration using partial parallel imaging with application to high spatial and temporal whole-brain fMRI. *Magn Reson Med* **63**, 1144-1153 (2010).

80. Caruyer E, Lenglet C, Sapiro G, Deriche R. Design of multishell sampling schemes with uniform coverage in diffusion MRI. *Magn Reson Med* **69**, 1534-1540 (2013).

81. Andersson JL, Xu J, Yacoub E, Auerbach E, Moeller S, Ugurbil K. A Comprehensive Gaussian Process Framework for Correcting Distortions and Movements in Diffusion Images. In: *ISMRM* (ed^(eds) (2012).

82. Sotiropoulos SN, *et al.* Advances in diffusion MRI acquisition and processing in the Human Connectome Project. *Neuroimage* **80**, 125-143 (2013).

83. Andersson JL, Skare S, Ashburner J. How to correct susceptibility distortions in spin-echo echo-planar images: application to diffusion tensor imaging. *Neuroimage* **20**, 870-888 (2003).

84. Smith SM, *et al.* Advances in functional and structural MR image analysis and implementation as FSL. *NeuroImage* **23**, 208-219 (2004).

85. Leemans A, Jones DK. The B-matrix must be rotated when correcting for subject motion in DTI data. *Magnetic Resonance in Medecine* **61**, 1336-1349 (2009).

86. Vos SB, Tax CM, Luijten PR, Ourselin S, Leemans A, Froeling M. The importance of correcting for signal drift in diffusion MRI. *Magn Reson Med* **77**, 285-299 (2017).

87. Dell'acqua F, *et al.* A modified damped Richardson-Lucy algorithm to reduce isotropic background effects in spherical deconvolution. *Neuroimage* **49**, 1446-1458 (2010).

88. Thiebaut de Schotten M, *et al.* Damage to white matter pathways in subacute and chronic spatial neglect: a group study and 2 single-case studies with complete virtual "in vivo" tractography dissection. *Cereb Cortex* **24**, 691-706 (2014).

89. Dell'Acqua F, Simmons A, Williams SC, Catani M. Can spherical deconvolution provide more information than fiber orientations? Hindrance modulated orientational anisotropy, a true-tract specific index to characterize white matter diffusion. *Hum Brain Mapp* **34**, 2464-2483 (2013).

90. Wassermann D, *et al.* The white matter query language: a novel approach for describing human white matter anatomy. *Brain Struct Funct* **221**, 4705-4721 (2016).

91. Abdi H, Williams LJ. Principal component analysis. *WIREs Comp Stat*, 433-459 (2010).

92. Thiebaut de Schotten M, *et al.* Rostro-caudal Architecture of the Frontal Lobes in Humans. *Cereb Cortex* **27**, 4033-4047 (2017).

bioRxiv preprint doi: https://doi.org/10.1101/372300; this version posted December 8, 2018. The copyright holder for this preprint (which was not certified by peer review) is the author/funder, who has granted bioRxiv a license to display the preprint in perpetuity. It is made available under aCC-BY 4.0 International license.

93. Parlatini V, *et al*. Functional segregation and integration within fronto-parietal networks. *Neuroimage* **146**, 367-375 (2017).

94. Kaiser HF. The varimax criterion for analytic rotation in factor analysis. *Psychometrika* **23**.

95. Chung F. *Spectral Graph Theory*. American Mathematical Society (1997).

bioRxiv preprint doi: https://doi.org/10.1101/372300; this version posted December 8, 2018. The copyright holder for this preprint (which was not certified by peer review) is the author/funder, who has granted bioRxiv a license to display the preprint in perpetuity. It is made available under aCC-BY 4.0 International license.

Supplementary materials

Supplementary Table 1. Terms selected for the study

acoustic	discriminative	insights	place	shifting
action	disgust	integrate	placebo	shifts
action observation	distance	integrated	placebo controlled	short term
actions	distraction	integrating	planning	signal task
addition	distractor	integration	pleasant	similarities
affective	distractors	integrative	pointing	similarity
ambiguous	distress	intelligence	position	size
anger	dorsal attention	intended	predict	skin
angry	duration	intention	predicted	sleep
anticipated	early visual	intentional	predicting	social
anticipation	eating	intentions	prediction	social cognition
anticipatory	economic	interference	prediction error	social cognitive
anxiety	effort	judgment	predictions	social interaction
appraisal	effortful	judgment task	predictive	social interactions
arithmetic	emotion	judgments	predicts	solving
arm	emotion regulation	language	preference	somatosensory
arousal	emotional	language comprehension	preferences	sound
articulatory	emotional faces	language network	preferential	sounds
association	emotional information	languages	preparation	space
associations	emotional neutral	learn	preparatory	span
associative	emotional responses	learned	primary auditory	spatial
attend	emotional stimuli	learning	primary motor	spatial attention
attended	emotional valence	learning task	primary sensorimotor	spatial information

bioRxiv preprint doi: https://doi.org/10.1101/372300; this version posted December 8, 2018. The copyright holder for this preprint (which was not certified by peer review) is the author/funder, who has granted bioRxiv a license to display the preprint in perpetuity. It is made available under aCC-BY 4.0 International license.

attending	emotions	letter	primary sensory	spatial temporal
attention	empathic	letters	primary somatosensory	spatiotemporal
attention task	empathy	lexical	primary visual	speaking
attentional	empirical	lexical decision	prime	speech
attentional control	encode	limb	priming	speech perception
attribution	encoded	linguistic	probabilistic	speech production
audio	encoding	listened	probability	speech sounds
audiovisual	encoding retrieval	listening	probe	speed
auditory	endogenous	long term	prospective	spoken
auditory stimuli	episodic	maintain	pseudowords	spontaneous
auditory visual	episodic memory	maintained	punishment	stimulus driven
autobiographical	error	maintaining	reach	stop signal
autobiographical memory	errors	maintenance	reaching	storage
automated	estimation	match	reactivity	strategic
automatic	executive control	matching	read	strategies
autonomic	executive function	matching task	reading	strategy
aversive	executive functions	memories	reappraisal	stress
avoid	expectancy	memory	reasoning	stroop
avoidance	expectation	memory encoding	recall	stroop task
awareness	expectations	memory load	recognition	subtraction
belief	expected	memory performance	recognition memory	success
beliefs	explicit	memory processes	recognition task	successful
believed	exploration	memory retrieval	recognize	suffering
bias	expression	memory task	recognized	suppression

bioRxiv preprint doi: https://doi.org/10.1101/372300; this version posted December 8, 2018. The copyright holder for this preprint (which was not certified by peer review) is the author/funder, who has granted bioRxiv a license to display the preprint in perpetuity. It is made available under aCC-BY 4.0 International license.

biased	expressions	memory tasks	recognizing	sustained
biases	external	memory wm	recollection	switch
binding	eye	mental imagery	rehearsal	switching
body	eye field	mentalizing	reinforcement	syntactic
calculation	eye fields	mnemonic	relational	tactile
capacity	eye movement	monetary	relevance	tapping
capture	eye movements	monetary reward	remember	target
categories	eyes	money	remembered	target detection
categorization	face	monitor	remembering	taste
category	face recognition	monitored	repeat	term memory
causal	face stimuli	monitoring	repeated	theory mind
choice	faces	mood	repetition	thinking
choices	facial	moral	repetition suppression	thought
choose	facial expression	motion	repetitive	thoughts
cognitive control	facial expressions	motivation	response inhibition	threat
cognitive emotional	familiar	motivational	response selection	threatening
coherence	familiarity	motor	responsiveness	time task
coherent	fear	motor control	retention	timing
color	fearful	motor imagery	retrieval	tom
combination	fearful faces	motor performance	retrieved	tone
combinations	feedback	motor response	reward	tones
combining	feeling	motor responses	reward anticipation	tool
communication	feelings	motor task	rewarding	tools
competing	finger	movement	rewards	touch
competition	finger movements	movements	rhythm	unfamiliar
comprehension	finger tapping	moving	risk	unpleasant
concept	flexibility	multisensory	risky	valence
concepts	flexible	music	rotation	valuable
conceptual	fluency	musical	rule	value

bioRxiv preprint doi: https://doi.org/10.1101/372300; this version posted December 8, 2018. The copyright holder for this preprint (which was not certified by peer review) is the author/funder, who has granted bioRxiv a license to display the preprint in perpetuity. It is made available under aCC-BY 4.0 International license.

conditioned	food	names	rules	values
conditioning	foot	naming	saccade	verb
conflict	form	navigation	saccades	verbal
conflicting	forms	negative emotional	sad	verbal fluency
congruency	gain	neutral faces	salience	verbal working
congruent	gains	neutral pictures	salient	verbs
congruent incongruent	gambling	neutral stimuli	search	video
conscious	game	nociceptive	secondary somatosensory	video clips
consciousness	gaze	nogo	seeking	videos
consolidation	gestures	noun	segregation	view
context	goal	nouns	selection	viewed
contexts	goal directed	novel	selective	viewing
contextual	goals	novelty	selective attention	violations
control processes	grasping	noxious	selectivity	virtual
coordination	hand	number	self	vision
covert	hand movements	numbers	self referential	visual
craving	hands	numerical	self reported	visual attention
cue	happy	object	semantic	visual auditory
cued	happy faces	object recognition	semantic information	visual field
cues	head	objects	semantic knowledge	visual information
decision	heard	observing	semantic memory	visual motion
decision making	hearing	oddball	semantics	visual perception
decision task	identification	oral	sensation	visual spatial
decisions	identity	order	sensations	visual stimuli
declarative	illusion	orientation	sensorimotor	visual stimulus
decoding	imagery	oriented	sensory	visual word
default mode	imagine	orienting	sensory	visuo

bioRxiv preprint doi: https://doi.org/10.1101/372300; this version posted December 8, 2018. The copyright holder for this preprint (which was not certified by peer review) is the author/funder, who has granted bioRxiv a license to display the preprint in perpetuity. It is made available under aCC-BY 4.0 International license.

			information	
default network	imagined	orthographic	sensory modalities	visuomotor
delay	imitation	overt	sensory motor	visuospatial
delayed	implicit	pain	sentence	vocal
demand	impulsivity	painful	sentence comprehension	voice
demanding	incongruent	passive viewing	sentences	voluntary
demands	index finger	personal	sequence	wm
depth	induction	personality	sequences	wm task
detect	inference	personality traits	sequential	word
detected	inferences	perspective	serial	word form
detecting	inhibit	phonetic	series	word pairs
detection	inhibiting	phonological	sex	word recognition
detection task	inhibition	photographs	sexual	words
digit	inhibitory	picture	shape	work
discrimination	inhibitory control	pictures	shapes	working memory
discrimination task	insight	pitch	shift	written

bioRxiv preprint doi: https://doi.org/10.1101/372300; this version posted December 8, 2018. The copyright holder for this preprint (which was not certified by peer review) is the author/funder, who has granted bioRxiv a license to display the preprint in perpetuity. It is made available under aCC-BY 4.0 International license.

Supplementary Table 2. Taxonomy of functional lateralisation

Maps	Principal Component label	RH > LH				LH > RH			
		# voxels	T value	MNI X, Y, Z	Anatomical area	# voxels	T value	MNI X, Y, Z	Anatomical area
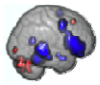	**Language**	911	18.05	12,-78,-34	Crus II	2947	42.03	-50,18,18	Prefrontal. C., extending into Precentral. G.
		45	12.45	28,28,50	Sup. Front S.	2607	40.59	-58,-42,6	Mid. Temp. G. (posterior) & Supram. G. extending into Fusiform C.
		28	12.41	32,-96,6	Occipital pole	160	20.59	-6,8,62	SMA (medial)
						102	18.03	-40,-60,24	Sup. Temp. S., (posterior, deep)
						98	15.71	-52,-8,-8	Sup. Temp. S. (middle-to-anterior segment)
	Movement	36	13.30	6,-56,-12	Area V	365	15.53	-40,-14,60	Precentral G. (middle part)
		23	12.24	18,-50,-28	Area VI	149	16.35	-10,-12,58	Border of Precentral G (medial) & SMA
						34	13.78	-10,-44,76	Border of Sup. Par. L. & Postcentral G.
	Eye movement	120	16.50	20,-64,52	Sup. Par. L., bank of Intra-Par. S.	322	19.04	-30,-48,56	Sup. Par. L.
		66	15.55	4,8,60	SMA (medial)				
		48	13.15	24,-8,52	Mid. Front. S, (posterior end)				
		25	13.77	24,-46,26	White matter				
		21	11.96	56,-40,38	Supram. G. (posterior)				
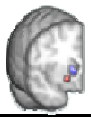	**Reward**	23	11.41	14,10,-8	Putamen (inferior)	66	20.03	-2,10,-2	Nucleus accumb.*
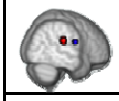	**Pain**	107	17.53	52,-30,24	Planum temporale	36	13.36	-62,-10,22	Postcentral G. (inferior)
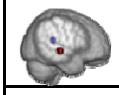	**Auditory**	60	11.90	58,-20,0	Sup. Temp. G. (posterior)	38	12.44	-48,-34,20	Planum temporale
	Action (observation)	74	14.48	62,-38,22	Supram. G. (posterior)	59	14.25	-24,0,66	Sup. Front. G., (posterior)
						40	13.33	-56,-22,38	Postcentral S. (inferior) & Supram. G. (anterior)
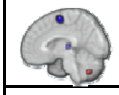	**(Finger) tapping**	54	13.02	14,-62,-44	Area VIIIb	93	16.36	-4,-6,60	SMA (medial)
						29	13.34	-10,-20,8	Thalamus (posterior)
	Calculation/numerical	25	13.01	40,-50,42	IPS (lower bank)	59	14.75	-36,-68,-38	Crus I
						35	14.14	-20,-58,56	IPS (upper bank)
	Phonetic/ Speech perception	47	14.01	48,-24,2	Sup. Temp. S. (posterior, deep)	56	12.98	-56,6,18	Precentral G.(inferior)
						20	11.68	-62,-28,4	Sup. Temp. G. (posterior)

bioRxiv preprint doi: https://doi.org/10.1101/372300; this version posted December 8, 2018. The copyright holder for this preprint (which was not certified by peer review) is the author/funder, who has granted bioRxiv a license to display the preprint in perpetuity. It is made available under aCC-BY 4.0 International license.

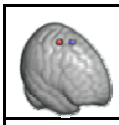	**(Motor) imagery**	27	12.60	34,-10,72	Precentral G.	21	12.50	-18,4,68	Sup. Front. G.
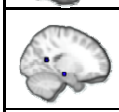	**Autobiographical (memory)**					26	14.33	-14,-52,16	Precuneus/anterior end of Par.-Occ. S.
						21	11.98	-22,-16,-14	Hippocampus
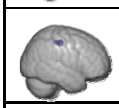	**Touch**					92	14.32	-34,-28,52	Postcentral G.
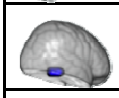	**Visual word/form**					498	24.20	-42,-42,-12	Fusiform cortex
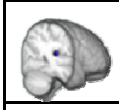	**Music**					36	12.36	-38,-26,18	Planum temporale
	Motor performance					21	12.42	-44,-56,-46	Crus II
	Facial expression	100	14.87	52,-44,4	Sup. Temp. S.(posterior)				
		27	11.96	34,2,-26	Amygdala (inferior)				
	Stop/ inhibition	196	17.84	24,52,34	Anterior segment MFSulc / frontal pole				
		88	13.41	18,16,68	Sup. Front.G.				
		58	13.58	48,22,-2	Pars opercularis (inferior)				
	Decision making	44	14.19	14,28,-20	Medial Orbital G. (posterior)				
	Working memory	54	13.61	32,12,54	Mid. Front G. (posterior)				
	Fearful (faces)	82	17.09	30,0,-14	Amygdala (superior)				
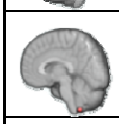	**(Un-) pleasant (faces)**	29	13.70	8,-50,-60	Area VIIIb				
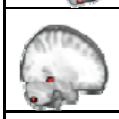	**Navigation**	50	12.70	36,-66,-50	Area VIIb				
		38	11.99	28,-36,-14	Parahippocampal G. & Fusiform C.				
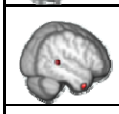	**Social interaction**	48	12.89	44,10,-38	Temporal pole				
		24	11.90	44,-44,8	Sup. Temp S. (posterior end)				
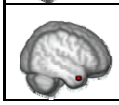	**Violations**	42	13.16	50,10,-30	Temporal pole				

bioRxiv preprint doi: https://doi.org/10.1101/372300; this version posted December 8, 2018. The copyright holder for this preprint (which was not certified by peer review) is the author/funder, who has granted bioRxiv a license to display the preprint in perpetuity. It is made available under aCC-BY 4.0 International license.

Supplementary Table 3. Principal components and the terms with highest loadings

Language		**Movement**		**Eye movement**	
language	1.24	movement	0.66	eye movements	0.63
semantic	1.24	motor	0.60	eye	0.61
words	1.21	primary motor	0.55	eye fields	0.53
word	1.12	hand	0.50	saccade	0.52
reading	1.11	sensorimotor	0.50	saccades	0.51
sentences	1.05	movements	0.50	eye movement	0.32
sentence	1.04	motor control	0.42	movements	0.27
phonological	1.03	finger	0.40	eye field	0.26
comprehension	1.01	index finger	0.39	gaze	0.21
lexical	0.82	primary sensorimotor	0.39	moving	0.20
Reward		**Pain**		**Auditory**	
reward	0.58	pain	0.80	auditory	0.65
monetary	0.56	painful	0.72	auditory visual	0.52
monetary reward	0.48	noxious	0.60	visual auditory	0.43
reward anticipation	0.46	nociceptive	0.46	sounds	0.34
anticipation	0.39	secondary somatosensory	0.38	auditory stimuli	0.31
rewards	0.37	somatosensory	0.35	audiovisual	0.26
motivation	0.29	sensation	0.19	visual	0.21
motivational	0.19	discriminative	0.18	sound	0.20
rewarding	0.19	affective	0.18	speech	0.18
gain	0.16	skin	0.16	phonological	0.18
Action (observation)		**(Finger) tapping**		**Calculation / numerical**	

bioRxiv preprint doi: https://doi.org/10.1101/372300; this version posted December 8, 2018. The copyright holder for this preprint (which was not certified by peer review) is the author/funder, who has granted bioRxiv a license to display the preprint in perpetuity. It is made available under aCC-BY 4.0 International license.

action	0.65	tapping	0.80	calculation	0.53
actions	0.58	finger tapping	0.78	numerical	0.48
action observation	0.56	finger	0.53	arithmetic	0.48
observing	0.31	motor	0.26	numbers	0.32
grasping	0.19	index finger	0.23	digit	0.26
tools	0.19	motor task	0.17	number	0.24
rehearsal	0.18	motor performance	0.15	subtraction	0.22
movements	0.17	sensorimotor	0.15	distance	0.15
tool	0.17	sequential	0.14	solving	0.14
motion	0.16	hand	0.14	size	0.13
Phonetic / speech perception		**(Motor) imagery**		**Autobiographical (memory)**	
phonetic	0.54	imagery	0.73	autobiographical	0.93
speech perception	0.50	motor imagery	0.63	autobiographical memory	0.82
speech	0.37	imagined	0.42	memories	0.49
articulatory	0.26	mental imagery	0.39	semantic memory	0.38
speech sounds	0.23	imagine	0.17	personal	0.33
phonological	0.21	motor	0.16	retrieval	0.25
acoustic	0.17	pointing	0.13	remembering	0.24
speech production	0.17	foot	0.13	semantic	0.22
listening	0.16	hands	0.11	self referential	0.22
covert	0.15	perspective	0.11	retrieved	0.21
Touch		**Visual word / form**		**Music**	
touch	0.53	visual word	0.73	musical	0.61
tactile	0.51	word form	0.63	music	0.60
somatosensory	0.50	orthographic	0.50	auditory	0.29
primary somatosensory	0.41	word recognition	0.42	listening	0.26

bioRxiv preprint doi: https://doi.org/10.1101/372300; this version posted December 8, 2018. The copyright holder for this preprint (which was not certified by peer review) is the author/funder, who has granted bioRxiv a license to display the preprint in perpetuity. It is made available under aCC-BY 4.0 International license.

secondary somatosensory	0.26	reading	0.38	pitch	0.20
multisensory	0.21	word	0.25	sounds	0.18
vision	0.18	words	0.24	sound	0.16
finger	0.15	phonological	0.22	acoustic	0.15
sensory	0.15	form	0.21	rhythm	0.15
hand	0.14	letter	0.21	timing	0.13
Motor performance		**Facial expression**		**Stop / inhibition**	
motor performance	0.58	expressions	0.65	signal task	0.68
motor task	0.34	facial expressions	0.62	stop signal	0.65
noxious	0.11	facial	0.61	response inhibition	0.60
numbers	0.10	facial expression	0.48	inhibition	0.54
motor	0.10	expression	0.43	inhibitory	0.46
arousal	0.09	emotional	0.28	inhibitory control	0.39
feedback	0.09	happy	0.24	inhibit	0.25
eyes	0.09	face	0.23	nogo	0.19
finger	0.09	faces	0.21	inhibiting	0.13
memory performance	0.09	disgust	0.20	successful	0.12
Decision making		**Working memory**		**Fearful (faces)**	
decision making	0.58	memory wm	0.76	fearful	0.61
decision	0.54	wm	0.73	fearful faces	0.56
choices	0.49	wm task	0.58	faces	0.39
choice	0.47	working memory	0.50	neutral faces	0.27
decisions	0.41	memory	0.28	happy	0.23
value	0.32	maintenance	0.26	face	0.23
risky	0.31	numerical	0.13	angry	0.23
choose	0.26	probe	0.13	happy faces	0.21

bioRxiv preprint doi: https://doi.org/10.1101/372300; this version posted December 8, 2018. The copyright holder for this preprint (which was not certified by peer review) is the author/funder, who has granted bioRxiv a license to display the preprint in perpetuity. It is made available under aCC-BY 4.0 International license.

rewards	0.21	spatial	0.12	emotional	0.20
gains	0.19	maintained	0.11	fear	0.18
(Un-)pleasant (faces)		**Navigation**		**Social interaction**	
unpleasant	0.65	navigation	0.76	social interaction	0.66
pleasant	0.65	virtual	0.48	social	0.31
feelings	0.18	spatial	0.21	social interactions	0.20
valence	0.13	executive functions	0.14	social cognition	0.16
affective	0.13	self	0.14	gaze	0.15
emotional	0.12	space	0.11	recall	0.13
sensation	0.11	observing	0.11	language network	0.13
aversive	0.11	binding	0.09	successful	0.13
neutral pictures	0.11	thinking	0.09	illusion	0.12
social cognition	0.10	orientation	0.09	attend	0.12
Violations					
violations	0.48				
moral	0.25				
game	0.22				
spontaneous	0.18				
mental imagery	0.16				
motivation	0.14				
syntactic	0.14				
sensation	0.13				
sensory information	0.13				
conflict	0.12				

bioRxiv preprint doi: https://doi.org/10.1101/372300; this version posted December 8, 2018. The copyright holder for this preprint (which was not certified by peer review) is the author/funder, who has granted bioRxiv a license to display the preprint in perpetuity. It is made available under aCC-BY 4.0 International license.

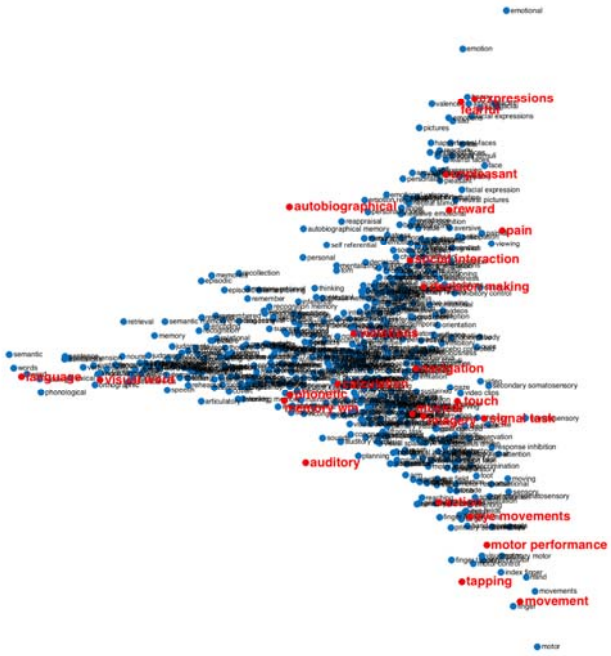

Supplementary Figure 1. Low dimensional structure of the functional lateralisation in the brain. Spatial embedding of all Neurosynth terms in two dimensions revealing a triangular organisation with 3 apices: symbolic communication, perception/action, and emotion.

bioRxiv preprint doi: https://doi.org/10.1101/372300; this version posted December 8, 2018. The copyright holder for this preprint (which was not certified by peer review) is the author/funder, who has granted bioRxiv a license to display the preprint in perpetuity. It is made available under aCC-BY 4.0 International license.

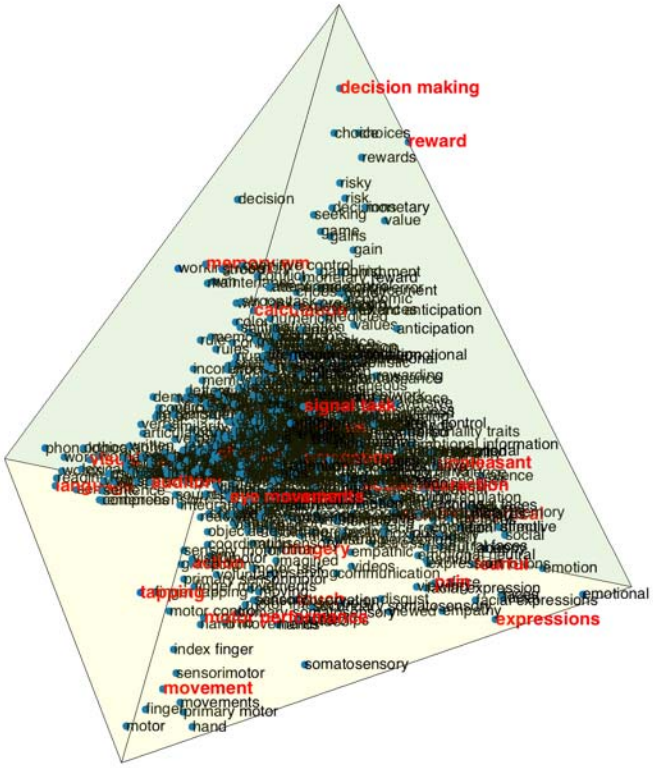

Supplementary Figure 2. Low dimensional structure of the functional lateralisation in the brain. Spatial embedding of all Neurosynth terms in three dimensions revealing a tetrahedron organisation with 4 vertices: symbolic communication, perception/action, emotion and decision making. (this is intended to be submitted as an interactive **3D file**)

bioRxiv preprint doi: https://doi.org/10.1101/372300; this version posted December 8, 2018. The copyright holder for this preprint (which was not certified by peer review) is the author/funder, who has granted bioRxiv a license to display the preprint in perpetuity. It is made available under aCC-BY 4.0 International license.

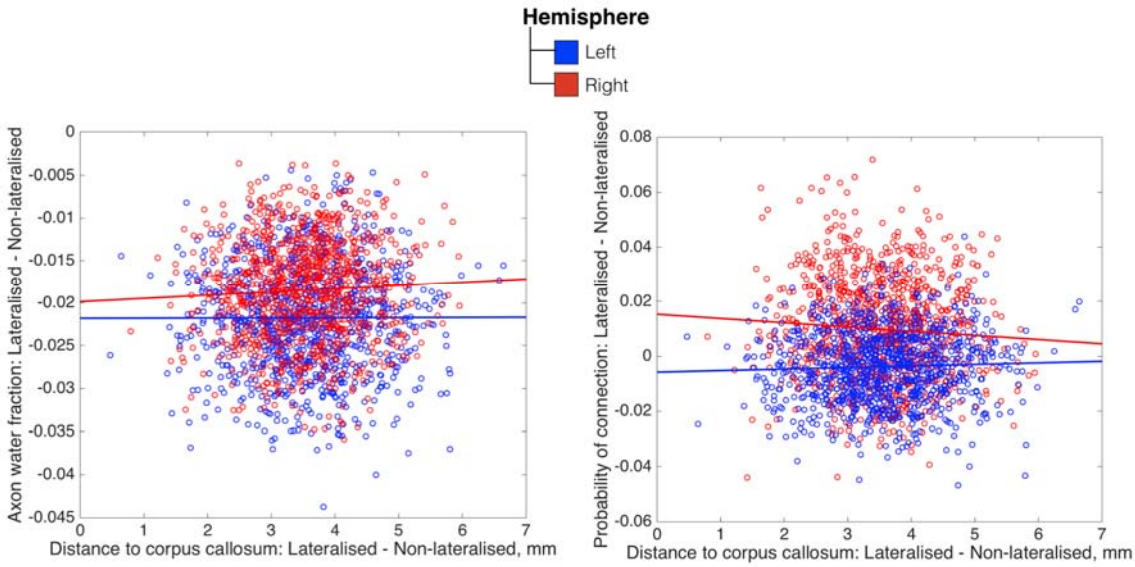

Supplementary Figure 3. Relationship between the two connectivity variables studied in the manuscript and the distance from the midsection of the corpus callosum.

bioRxiv preprint doi: https://doi.org/10.1101/372300; this version posted December 8, 2018. The copyright holder for this preprint (which was not certified by peer review) is the author/funder, who has granted bioRxiv a license to display the preprint in perpetuity. It is made available under aCC-BY 4.0 International license.

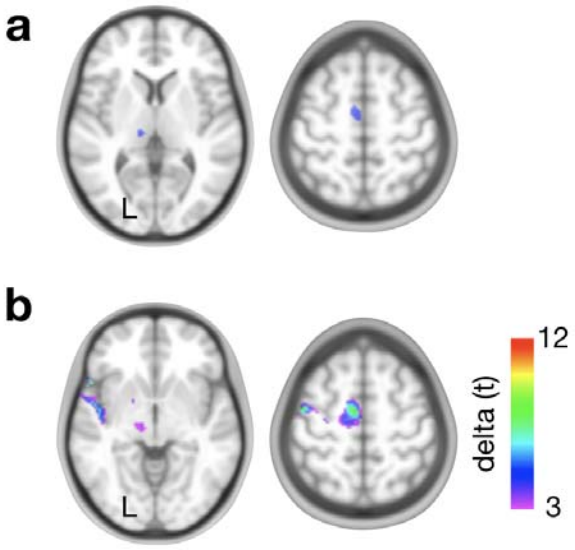

Supplementary figure 4: Validation of the functional asymmetries derived from the meta-analysis of functional MRI with raw functional MRI results derived from a finger tapping task in 142 right-handed participants (Tzouriot-Mazoyer et al. Front Hum Neurosci. 2015). a) functional lateralisation map for finger tapping task derived from the meta-analytic approach b) Subtraction between left-hand and left-right flipped right-hand finger tapping symmetric functional MRI maps.

bioRxiv preprint doi: https://doi.org/10.1101/372300; this version posted December 8, 2018. The copyright holder for this preprint (which was not certified by peer review) is the author/funder, who has granted bioRxiv a license to display the preprint in perpetuity. It is made available under aCC-BY 4.0 International license.

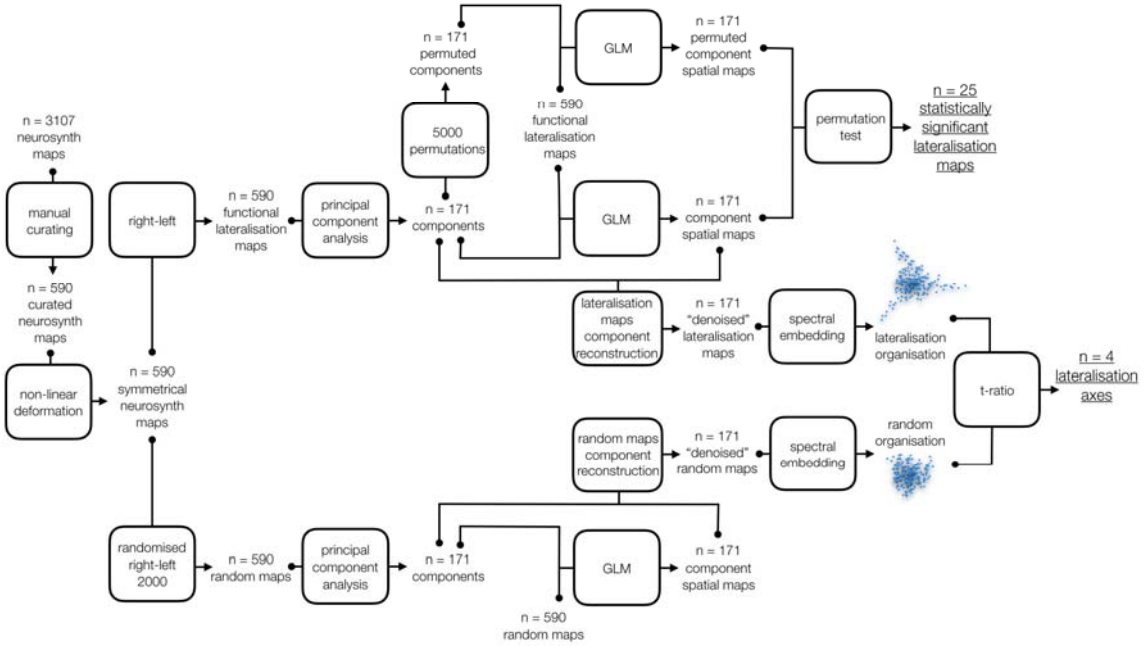

Supplementary Figure 5. Graphical summary of the global structure of functional lateralisation methods

bioRxiv preprint doi: https://doi.org/10.1101/372300; this version posted December 8, 2018. The copyright holder for this preprint (which was not certified by peer review) is the author/funder, who has granted bioRxiv a license to display the preprint in perpetuity. It is made available under aCC-BY 4.0 International license.

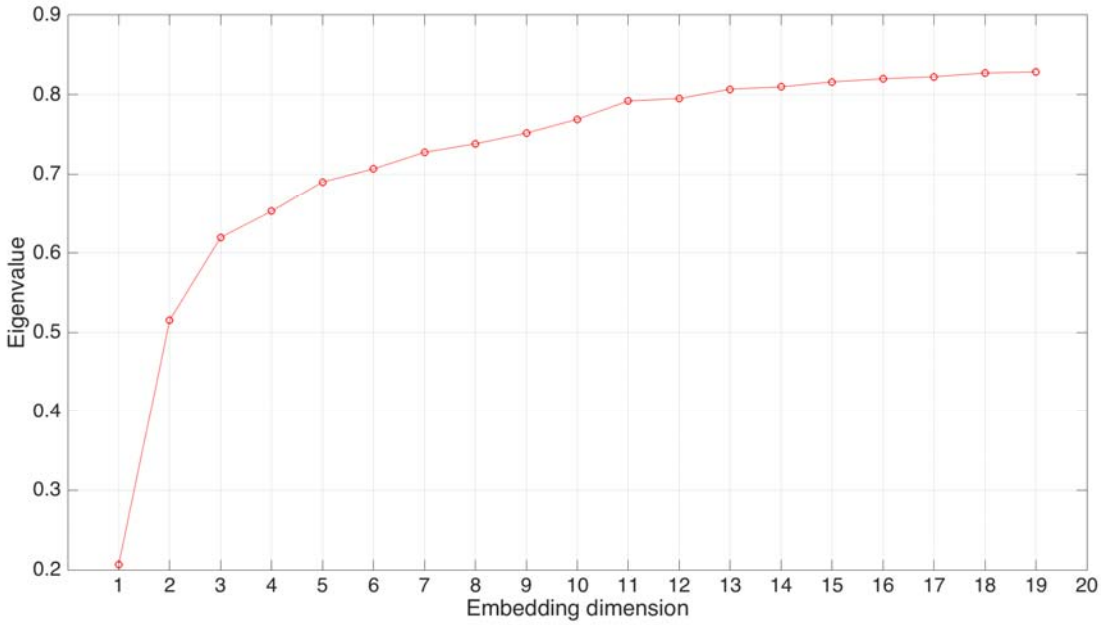

Supplementary Figure 6. Eigenvalues of graph Laplacian embedding

bioRxiv preprint doi: https://doi.org/10.1101/372300; this version posted December 8, 2018. The copyright holder for this preprint (which was not certified by peer review) is the author/funder, who has granted bioRxiv a license to display the preprint in perpetuity. It is made available under aCC-BY 4.0 International license.

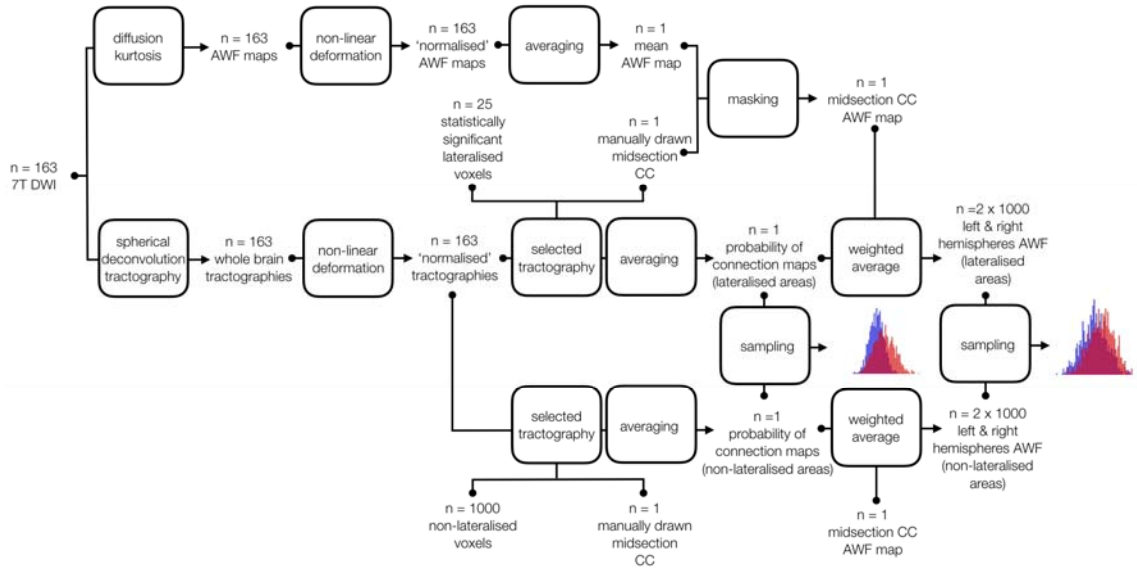

Supplementary Figure 7. Graphical summary of the analyses of function-structure relationship.